Fabrication of Fluorescent Nanoprobes and Their Applications in Nanophotonics

YAOSHUN JIA

Thesis submitted to the faculty of the Virginia Polytechnic Institute and State University
in partial fulfillment of the requirements for the degree of

Master of Science
In
Electrical Engineering

Yong Xu, Committee Chair
AnboWang
Kathleen Meehan

December 10, 2008
Blacksburg, Virginia

Keywords: Fluorescence, Nanoprobe, Quantum Dots, Image sensor, fiber taper

Fabrication of Fluorescent Nanoprobes and Their Applications in Nanophotonics

YAOSHUN JIA

ABSTRACT

In recent years, nanoprobe-based devices have attracted significant attention and found a wide range of applications, including nanostructure imaging, single molecular detection, and physical, chemical, and biological sensing applications. However, since the scale of nanodevices is substantially less than the optical diffraction limit, their fabrication remains a difficult challenge. Despite significant efforts, most of the fabrication techniques developed so far require expensive equipment and complicated processing procedures, which has hindered their applications.

In this thesis, we developed a new class of fluorescent nanoprobes consist of a silica fiber taper, a single carbon nanotube, and nanoscale fluorescent elements (such as semiconductor quantum dots). This nanoprobe provides a natural interface between the nanoscale structures (i.e., the fluorescent elements) and the microscale structure (i.e., the fiber taper), which can significantly simplify their fabrication. Furthermore, since the nanoscale fluorescent elements are produced through bottom-up processes such as chemical synthesis, we can easily tailor the functionalities of such fluorescent nanoprobes to many different applications in nanophotonics, including near field imaging, nonlinear optics mapping, and quantum electrodynamics.

We have custom designed an optical system for this nanoprobe fabrication. We have characterized the nanoprobes using transmission electron microscope (TEM) and scanning electron microscope (SEM) and performed preliminary experiments on near field scanning. Our current fabrication/imaging systems can be readily upgraded to achieve more advanced applications in nonlinear optics and quantum optics.

Acknowledgements

I am so grateful for the opportunity to come and study here at Virginia Tech and work in Center for Photonic Technology. I would like to express my most sincere gratitude to my advisor Dr. Yong Xu for giving me this opportunity to come here working on the topic I am interested in. Thanks for his generous support and freedom to accomplish challenges during project; thanks for his inspiring discussion. I would also like to thank other committee members, Dr. Anbo Wang and Dr. Kathleen Meehan for serving as my committee and valuable help and suggestions on my research and thesis. I would like to thank Dr. Anbo Wang for his encouragement, suggestions, friendship, wisdom, and providing me, also all other CPT members, such a nice lab environment; thanks to Dr. Kathleen Meehan for providing me sample, helping me to solve my experiment problems during the project and valuable suggestion on my thesis writing.

A special thank goes to our collaborator Dr. Zhiwen Liu, and his student Haifen Li, Kebin shi, Peng Li, and Qian Xu in Penn State University, for their assistance in my research topic and weekly video discussion on the projects.

I would like to thank my group members who ever worked with me: Yan Yin, Xiangyu Wei. I would like to also extend my thanks to all the faculty, staff and students in Center for Photonics Technology for their friendship, technical discussions, and support. My special gratitude also goes to Dr. Xiaopei Chen, Dr. Ming Han and his family, Yan Xi and their daughter Stephanie, for their friendship, warm heart and help. My thanks also go to all my friends here at Center for Photonics Technology, including those former members Dr. Yizheng Zhu, Dr. Fabin Shen, Dr. Xingwei Wang, Dr. Zhenyu Huang, Dr. Yongxin Wang and the current members, Bo Dong, Evan Lally, Jiajun Wang, Cheng Ma, , Yunmiao Wang, Yunjing Wang and Matt Hofmann and Jihaeng Yi.

Finally I would like to express my gratitude to my deepest love to my parents who trust me support me with their great love.

Contents

List of Figures

1 Introduction

1.1 Overview for the nanotechnology

In 1959, Nobel Laureate Richard Feynman gave a famous seminar, "There's Plenty of Room at the Bottom", in which he talked about the theory and principles of what is now commonly referred to as nanotechnology and how it could generate enormous technical impact and significantly change our world. His seminar marked the birth of nanotechnology, commonly defined as devices and technological developments at the scale of 0.1 to 100 nm, where new physical, chemical and biological properties appear and can significantly deviate from those of bulk materials. One of the first nanofabrication experiments was demonstrated in 1990, where IBM research lab deposited xenon atoms onto a nickel substrate to spell the "IBM" logo [1]. Since then on, research on nanotechnology has expanded significantly and has become one of the most important technological breakthroughs in the last two decades.

Although still far from mature, the advance in nanotechnology has created tremendously new opportunities. The development of nanomaterials, which include examples such as nanowires and quantum dots [2-6], allows us to control the size, surface and morphology of the novel materials and can lead to significant enhancement in the electrical, optical and chemical properties of such materials. A few examples are the enhanced mechanical properties of carbon nanotube [7, 8] and size-dependent fluorescence of quantum dots [9, 10]. Fluorescent nanomaterials have found a wide range of biological applications that require the labeling and tracking of single molecules [11]. Two examples are the fluorescent labeling of individual neurons in neurological systems [12] and green fluorescent protein (GFP) and its variants in transgenic animals [13, 14].

1.2 Nanoprobe

A nanoprobe is an optical device fabricated by tapering an optical fiber to nano scale. In engineering, nanoprobes have found many applications ranging from nano-radios to nano-sensors [15]. For example, carbon-nanotube-based nano-antennas have been

demonstrated for wireless communications in the THz and GHz frequency range. A key advantage of such nano-antennas is the high conductivity of the nanotubes, which have been measured to be approximately twice of the copper [16]. Another interesting nano device fabricated with a single carbon nanotube is the Nano Radio [17], where by using frequency and amplitude modulation, the nanotube radio has successfully received music in the commercially relevant 40-400 MHz range. The nanotube can be used simultaneously as all essential components of a radio: antenna, tunable band-pass filter, amplifier, and demodulator. Of particular interest is the needle-like geometry of the carbon nanotube, which can concentrate the electric field and demonstrate good field-emission properties.

For most of the nanodevices in the literature [18-22], their nanoscale sizes, unique geometries, and improved physical properties have created numerous advantages that cannot be easily achieved otherwise. However, the complexity of nanofabrication often presents a difficult challenge in full realizing these advantages. In the following section, we provide a brief summary of common nanofabrication techniques in the currently literature.

1.3 Near-field Scanning Optical Microscopy

Near-Field Scanning Optical Microscopy (NSOM) is a scanning nanoprobe technique that overcomes the diffraction limit in optics [23]. The most critical element in a NSOM system is the NSOM tip, which is formed from a small aperture at the end of a silica fiber tip and is defined by a layer of metallic coating. The ultimate resolution of NSOM system is limited by the aperture size of the NSOM tip, which has currently leveled out at the value of about 50 nm [24, 25].

The fundamental principle underlying the near field scanning optical microscopy (NSOM) is that the radiation through the aperture and into the region beyond the screen is collimated to the aperture size rather than to the wavelength of the radiation. The aperture based NSOM principle is illustrated in Figure 1-1, in which a cell membrane is placed within the near-field region to an aperture. The aperture acts as a light source and

can be scanned over the object. A detector was used to collect the light to generate a high-resolution image.

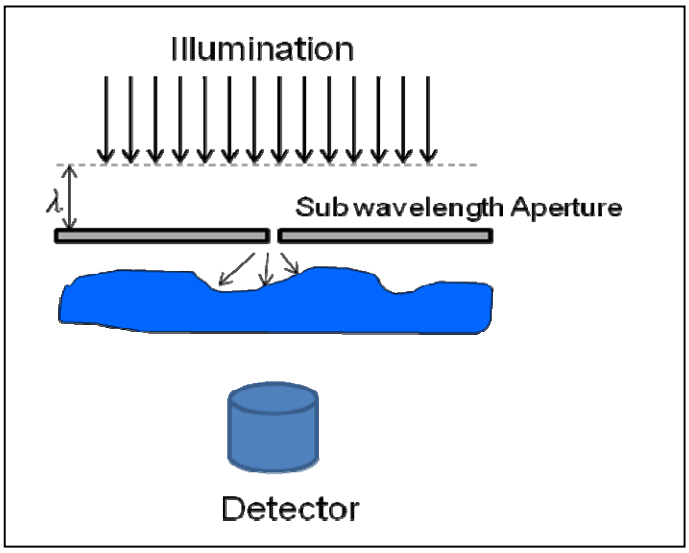

Figure 1-1: Scheme of aperture based NSOM system.

The interaction of light with an object results in the generation of both near-field and far-field light components. The far-field light propagates through space in an unconfined manner and is used in the imaging of conventional microscopy. The near-field light is non-propagating that exists only near the surface of an object at distances less than a wavelength of the light. Light in the near-field carries more high-frequency information and has its greatest amplitude in the region within the first few tens of nanometers of the specimen surface. The near-field light decays exponentially within a distance less than the wavelength of the light, it usually goes undetected. In effect, as the light propagates away from the surface into the far-field region, the highest-frequency spatial information is filtered out.

1.4 Carbon Nanotubes

In our project, we use carbon nanotubes (CNT) as part of the materials composed our nanoprobes. Carbon atoms have good mechanical properties and have been used in AFM tips for high resolution imaging, in which CNTs do not break when bent at large angles.

There are four allotropes: amorphous carbon, diamond, fullerene (C_{60}) and graphite sheet. Carbon nanotubes (CNTs) are formed by sheets of graphite in cylinder shape with hexagonal lattices of carbon atoms. Carbon nanotubes were first discovered by Sumio Iijima in 1991 [26]. Chemical vapor deposition (CVD), laser ablation and fused salt electrolysis methods have been used to produce CNTs. There are two main types of carbon nanotubes: single walled carbon nanotuebs (SWCNT) and multiwalled carbon nanotubes (MWCNT). Single-walled nanotubes (SWNTs) consist of a rolled single graphite, wrapped into a cylindrical shape. Multiwall nanotubes (MWNTs), as indicated by the name, consist of multi single wall carbon nanotubes, rolled layer by layer in the concentric circles as tree trunk. In Fig. 1-2, we show the field emission SEM image of multiple MWCNT on a silicon wafer. The diameters of these MWCNT, which are prepared through CVD growth, are 147 nm

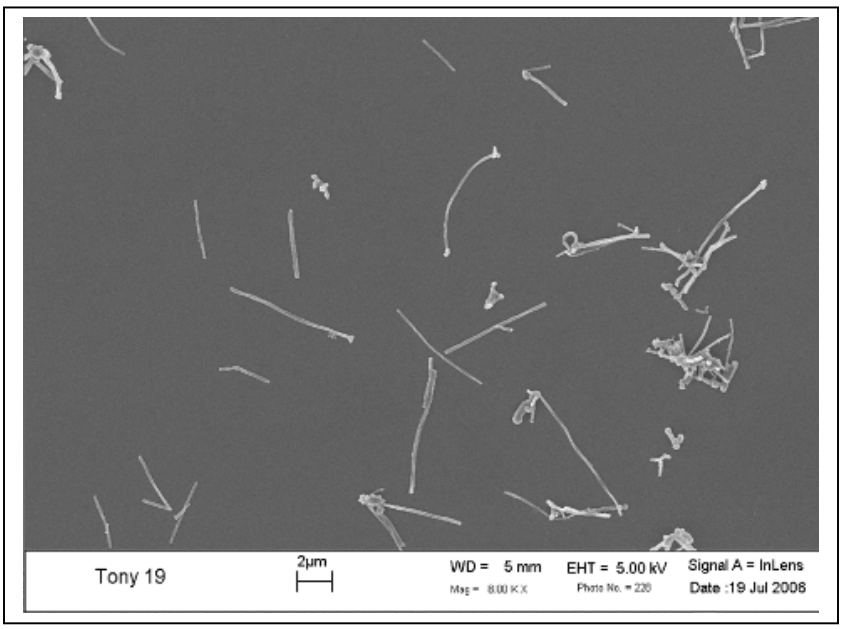

Figure 1-2. FESEM image for the MWCNT we used in nanoprobe

The electronic property of a CNT is highly structure dependent. MWCNTs are all metallic and SWCNT is either metallic or semiconducting, depending on the rolling angle of the carbon the sheets. All “armchair”-shaped SWCNTs are metallic and zigzag-shaped SWCNTs are semiconducting. A pair of integers (n, m) is used to denote the

nanotube type [27, 28]. The nanotube is either of the armchair ($n = m$), zigzag ($n = 0$ or $m = 0$), or chiral (any other n and m). If $n - m = 3k$, where k is a nonzero integer, this will be a semiconducting SWCNT with a tiny band gap while all other SWCNT are semiconductors with a band gap that inversely depends on the nanotube diameter [84,85].

The one-dimensional electronic structure enables metallic CNTs to carry high currents with small heating [29, 30], so the electronic transport could carry electron over long lengths without scattering. The thermal conductivity of an individual MWNT is around 3000 W/m*K at room temperature, which is greater than that of diamond and graphite (both 2000 W/m*K) [31]. Phonons also propagate easily along the nanotube.

CNTs also show great mechanic properties. SWNTs are stiff with high Young's modulus and high tensile strength, which is unmatched by any other known materials. CNTS are also extremely elastic. They can bend to very large angles. The calculated Young's modulus for an individual (10, 10) nanotube is 0.64 TPa [32]. SWCNT could be extended elastically by 5.8% before breaking. The calculated strain and modulus is 37 GPa [33, 34], which is close to the maximum strength of silicon carbide nanorods (53 GPa) [35]. Because of these impressive mechanic properties and light weight, CNTs have a lot application in light structural materials. The density-normalized modulus and strength of this SWCNT are 19 and 56 times bigger than steel wire and 2.4 and 1.7 times larger than silicon carbide nanorods [35].

Carbon nanotubes become good candidate in the nanoprobes application in high resolution imaging, nano-lithography, nano electrodes because of their small sizes, high conductivity, high mechanical strength and elasticity. The nanotube-based field emitting devices have been already fabricated by industries for demonstration on flat HDTVs. Single MWNT attached to the end of AFM tip and scanning probe microscope tip for imaging has already been reported [36]. Metallic CNTs can be used in STM, AFM instruments and electrostatic force microscope. The advantage of the nanotube tip is its high aspect ratio so it can be used in imaging small, deep surface cracks, which is difficult for AFM tip which use the larger, blunter etched Si or metal tips. In addition,

nanotubes are highly elastic so they would buck instead of break or crash on contact with the substrates. And this bucking is reversible on retraction of the tip from the substrate.

In addition to applications in high resolution imaging in near field scanning microscope and tapping mode of AFM, carbon nanotubes were also used as active tools for surface manipulation. For example, a pair of nanotubes were positioned appropriately on an AFM tip and controlled by applying voltage to use this two-tube nanoprobe as nano tweezers to pick up and release nanoscale structures on surfaces [37].

1.5 Quantum Dots

Quantum Dots are semiconductor nanocrystals with diameter from 1nm to 10 nm, which have large surface area to volume ratio and three dimensional spatial confinement effects. When the nanoparticles' size is smaller than the Bohr radius of the bulk semiconductor, quantum confinement appears. Due to the 3D quantum confinement, the energy levels of the excited carriers become discrete. In the particular case of cadmium sulfide (CdS) and cadmium selenide (CdSe) semiconductor nanocrystals, the size dependence of the fundamental electron-hole state, E_{1S1s}, can be described by the Equation (1): [38]

$$E_{1S1s} = E_g + \frac{\pi^2 h^2}{2a^2 \mu} - 1.786 \frac{e^2}{\varepsilon a} \qquad (1)$$

a is the particle radius, μ the electron-hole reduced mass, e the electronic charge and ε the dielectric constant of the bulk semiconductor. The first term on the right, E_g, corresponds to the bulk band gap energy, the second term accounts for the confinement energy and the third term for the electron-hole Coulomb interaction.

Equation (1) shows that, besides inducing energy quantization, decreasing the dots size makes the Coulomb term shift the total energy to lower values with a a^{-1} dependence. While the three dimensional confinement term adds to the total energy with a a^{-2} dependence. This way, for smaller dot sizes, the confinement term becomes dominant and the optical spectrum shows a blue shift in the band edge energy when the QD's size

is decreased below Bohr radius a_B. The smaller the dot, the greater the blue shift will be. From Equation (1), we can see that quantum dots' band gap can be tuned by control of the quantum dots' size (a) or material type (ε).

Due to the size distribution of quantum dots, the emission spectrum of quantum dots was broadened, since a colloidal dispersion the solid particles cannot have exactly the same size. The emission of a QD is related to its size, the slight differences in size result in variations in the emission wavelength. As a consequence, the emission spectrum will be much broader than the individual QDs spectra. At present, it is possible to achieve size distributions with variation lower than 5%, which will cause the full widths at half maximum (FWHM) of the spectrum to approximately 25-30 nm broader. This is quite narrow in comparison to the spectral response of many luminescent dyes.

1.6 Nano Fabrication

Nanofabrication methods can be roughly divided roughly into two groups: the top-down and the bottom-up methods [39]. Top-down methods start with patterns made on a larger scale and then reduce their lateral dimensions before forming nanostructures. On the other hand, bottom-up methods begin with atoms or molecules to build up nanostructures, in many cases through smart use of self-organization.

Top-down approaches are good for producing structures with long-range order and for making macroscopic connections. The bottom-up approaches are best suited for assembly and establishing short-range order at nanoscale dimensions. The integration of top-down and bottom-up techniques can significantly expand the possibilities of nanofabrication.

1.6.1 Top-down

The top-down methods for nanofabrication [40] could be broadly subdivided into 3 categories: (a) chemical fabrication; (b) laser machining; and (c) mechanical processing;

Chemical vapor deposition (CVD) [41], chemical milling and photochemical milling are the major three chemical fabrication methods. Chemical milling removes material by etching of preferentially exposed surface to get clean, sharp, well defined edges with mask. Photochemical milling used lithography method to etch desire the materials. Photochemical milling and chemical milling are both isotropic and etching speed is low.

Laser machining is now commonly used in industry for sheer cutting, welding and drilling. Laser machining was first introduced into micromachining in 1982 by IBM researcher R. Srinivasan and V. Mayne-Banton [42]. They used short optical pulse produced by an ultrafast laser to do the cutting and removing materials.

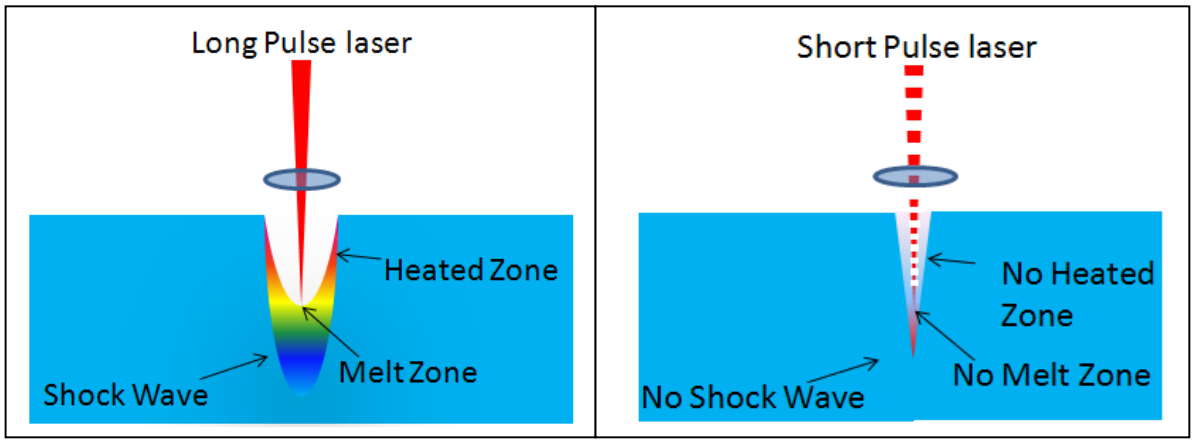

Figure 1-3: (Left) Long-Pulse Laser-Matter Interaction; (Right) Ultrafast Pulse Laser-Matter Interaction.

According to the laser properties, laser machining can be divided into three types: CW (continuous wavelength), short pulse, and ultrafast laser. CW laser is commonly used laser for melting and welding. Short pulse laser is usually the laser with pulse longer than 10 ps. Ultrafast laser is also called femtosecond laser, which indicate that the pulse of the laser is usually in fertosecond. Short pulse laser could vaporize the substrate without vacuum condition. Ultrafast laser could concentrate much energy at so fast rate that force materials to generate plasma directly from solid state to gas state. The different effect of short pulse and ultra short pulse laser micromachining is show in Figure 1-3 above [42].

Mechanical processing has been designed to operate on materials with desired structure, surface and shape. There are several mechanical machining methods: ultra-high-precision mechanical machining, ultrasonic machining, abrasive water jet machining and focused ion beam milling. In ultra-high-precision mechanical machining, it is required to control the temperature, vibration to achieve the high accuracy. The accuracy for ultra-high-precision machining reached 1nm in year 2000. Ultrasonic machining uses high frequency vibration to abrasive and make accurate cavity. Ultrasonic machining is most effective for hard and brittle materials, not for soft materials, since soft materials would absorb vibration energy and undergo thermal expansion. Water jet abrasive machining cut material at room temperature, so there is no thermal expansive or stress on the material. Focused ion beam techniques (FIB) use a stream of energetic ions to cut and remove materials. By magnetic lens focus, the ion stream diameter can be reduced and focused down to submicron, even 50 nm now. But the etching rate is slow and it is expensive. A good example of FIB technology was the single electron transistor (see figure 1-4), on which researchers controlled the ion beam to etch two trenches with widths of 15 nm as tunneling barriers to form the gate, drain and source region on one carbon nanotube [43].

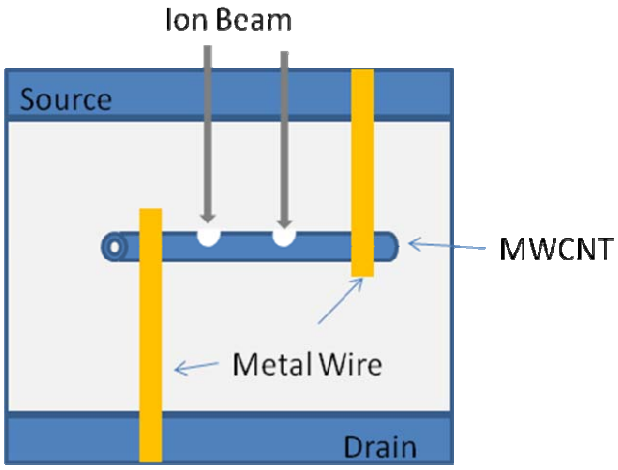

Figure 1-4. Scheme of nanotube SET fabricated by using FIB.

1.6.2 Bottom-up

Bottom-up nanofabrication relied on the chemical and physical interaction among atoms and molecules to arrange them into structures with nanoscale features. Inspiration for bottom-up approaches comes from biological systems, where nature has harnessed chemical forces to create essentially all the structures needed by life. For example, from study on the AFM structures of butterfly's eyes, researchers found that it was the nipple structure that offered outstanding optical and wetting ability properties, which had technical applications in the area of antireflective coatings [44, 45] and self-cleaning of super hydrophobic structures [46 - 49].

In industry, top-down technology is the dominant method for device fabrication, but when the device size goes to less than 10nm or around 1nm, bottom-up approaches play an increasingly important complement method to top-down techniques [50, 51]. Recently, researchers began to use bio materials (DNA, protein, virus, et. al) as soft template to make one dimensional, two dimensional, and three dimensional nanostructure. DNA is a special molecular with complementary molecules. DNA and its complementary molecular could recognize each other [52–56]. One dimensional silver nanowire was synthesized by DNA as stabilizer and template via self-assembly [57]. Protein system also has complementary protein molecular recognition and combination functions. Mann and his group used protein to form the Au nanoparticle self-assembly under antibody/antigen and streptavidin/biotin recognition [58]. Virus assisted self-assembly depends strongly on the virus structures and assembly process. Nanowires of metals, semiconductors and magnetic materials had been fabricated using rod-shape virus such as M13 bacteriophage and tobacco mosaic virus [59, 60].

Other bottoms up synthesis methods, such as epitaxy, biomimetic assembly, are also used frequently. Epitaxy could deposit single crystal structures one atomic layer at a time [61, 62]. Biomimetics was defined as man-made processes, or systems that imitate nature [63]. A recent successful research in the biomimetics was the study on the nano structure of osculum on geckos' toes [64]. They duplicate gecko's toe hairs to dense array of

plastic fibers, with spacing of 1.6 μm between each other, diameter of 500 nm, and length of 2 μm. This optimized structure achieved an adhesion force of 3 N/cm^2, almost 30% that of the real gecko. This adhesion strength would be sufficient to suspend a man with just adhesive gloves covering his palms.

1.7 Application of Nanoprobes

There has been an increasing demand for instruments that can provide low-cost and rapid sensory information. The ultimate aim of the fabrication of nanoprobes is to develop high performance sensors for bio/chemical/thermal/mechanic signal detection. Nanofabrication could make sensor systems smaller, cheaper and portable, which could be interesting for embedded system in real time monitoring and 'point of care' diagnostics.

1.7.1 Chemical Sensing

Chemical sensor was first invented as far as more than 200 years ago: in 1784, Lavoisier detected CO in the exhaled breath of guinea pigs [64]. Later, colorimetric assays and gas chromatography columns were used to detect trace amount of gas and analyze the component [66]. The need to determine the chemical composition of smaller and smaller volumes has led to the development of nanoscale sensors, some of which rely on the use of nanoprobes [67].

An successful nanodevice is the PH sensor, which had good temporal resolution, were inexpensive, simple to use and had high sensitivity. The sensor functioned by measuring the surface fluorescence of single cell after loading the cell with a pH-sensitive fluorescent dye CFDA (*5 (6)-Carboxyeosin diacetate*) [68]. The sensors had submicrometer in dimension and had excellent detection limits and millisecond response times, which had applications in intracellular and intraembryonic measurements [69].With this submicrometer optic fiber sensor and near-field photopolymerization, we

could do the reduce the sample amount to a million fold or more, while simultaneously use at least a hundred fold time.

1.7.2 Bio/Medical Sensing

A nanobiosensor is a biosensor with dimensions on the nanometer scale. Various elements can be used in biosensing, such as biological molecular species (antibody, enzyme, protein, or a nucleic acid) or a living biological system (cells, tissue, or whole organisms).The basic theory is a biochemical mechanism for recognition.

The first application of antibodies in biosensor was an experiment, which used fiber optic immune sensor for in situ detection of the chemical carcinogen benzo[a]pyrene (BaP) [70]. This was an important advance since it was the first sensor that monitored in vivo biological processes within single living cells using biosensor, which could greatly improve our understanding of cellular function [71].

With the advantage of small size, biocompatibility and easy fabrication, fiber optic sensors attract considerable interest among researchers. Extensive researches and studies were carried out with fiber optic sensors that can be inserted into biological cells and allow intracellular sensing. [72-76]. Tip diameters of the fiber typically range between 20 and 100 nm, which is small enough to be inserted into a single cell.

1.7.3 Thermal Sensing

One of the many interesting properties of fluorescence is its strongly temperature-dependence effect. For example, erbium/ytterbium co-doped fluoride fiber possesses multiple absorption and emission lines. Two erbium emission lines, at 520nm and 550nm, are in thermal equilibrium, where the ratio of relative integrated intensity from each radiative transition directly depends on the temperature. Their relationship can be described by a law of the following form [77]:

$$I_{520} / I_{550} \propto e^{-\Delta E / kT}$$

I_{520} and I_{550} are the intensities of the two fluorescence lines at 520 nm and 550 nm, respectively. ΔE is the energy gap between these two levels. k is Boltzmann's constant and T is the ambient temperature in Kelvin. If we measured the intensity of each spectrum, we could derive the temperature since ΔE is constant which is determined by materials.

To study the temperature dependence, researchers use 975 nm anti-strokes excitation process to get the FL spectrum of the erbium/ytterbium co-doped fluoride glass [78]. They used this nanoprobe to scan devices to get the surface information. And it is surprise that this thermal scanning nanoprobe works pretty well to reveal the surface detail at micro or nano scale.

1.7.4 Other Applications

There are some applications of nanoprobe, such as mass sensing, fluid speed, surface stress / tensile sensing. A majority of these nanosensors use cantilever beams as substrates of the nanosensor. The sensing principle is based on piezo-electronics.

1.8 Motivations

Though nanotechnology has great advances in recent, we still have very little method to visualize and image nanostructures. For example, SEM and TEM were invented long time ago. Almost 50 years passed, SEM and TEM are still the major two available methods we can used to observe nanomaterials and nanostructures. There are a lot of spaces in this area that need more focused research to develop new powerful method and instrument to image the nano structures in closer detail and also, easier, and less expansive.

As overviewed above, fluorescence optic fiber nanoprobe aroused our great interest since they may have multifunctional application in bio sensing, temperature sensing and many

other application, especially, sub wavelength imaging, which can be developed into new system to image the nano structures. Much research work has been done in the sub-wavelength imaging. For example, near field scanning optical microscope (NSOM) [79, 80]. In NSOM, a metal coated optic fiber tip with a small aperture is used to collect the near field evanescent wave to obtain the surface information. The ultimate resolution of any NSOM system is limited by the aperture size of the NSOM tip, which has currently leveled out at the value of ~50 nm. There are also many issues associated with the aperture-less tips, such as heating, artifacts, contrast, sensitivity, topology and interference with surface.

To overcome these problems, we proposed to make a fluorescence nanoprobe, which uses the single carbon nanotube as the sensor tip. The fluorescence material that we will use is a quantum dot, which is a semiconductor crystal of small uniform size with bright, stable, tunable wavelength fluorescence and high quantum efficiency. This nanoprobe could be used in non-perturbed ultrahigh resolution near-field imaging, vacuum field image and as a single photon source [81-83].

1.9 Organization of Thesis

In this dissertation, the first chapter gives a brief overview on the nanotechnology, including the history review, nanofabrication method and classification, nanoprobe application and motivation.

Chapter 2 describes the fabrication method and process. This chapter included all the structure and processing details of our nanoprobe. It will provide the details of chemical procedure used to make modifications on the surface of quantum dots, and how to attach these QDs to the silica nanospheres via covalent bonding. Also, in this chapter, two methods used to make optical fiber tapers, and the nano-manipulation of the single multiwall carbon nanotube to these tapers to make sensor tip in our nanoprobe.

Chapter 3 describes the system design on how to set up the stages to make it possible and easy to manipulate these tiny nanoscale nanoprobes. Also in this chapter, the integrated

detection system with liquid nitrogen cooled photodetector to measure the signal of the interested area will be described.

Chapter 4 is the last chapter that summarizes the major result and contributions of our project. In this chapter, we also review the problems that need to improve the sensor, to be solved later; Last, we will predict the future development of our nanoprobe and system.

2 Fluorescence Nanoprobe Fabrication

2.1 Introduction

Subwavelength imaging, which allows us to visualize optical near field with nanoscale resolution, is a critical component of nanotechnology. The demonstration of sub wavelength imaging, however, is quite difficult due to optical diffraction, the spatial resolution of traditional optical microscopy is limited to $\lambda/2$, where λ is the optical wavelength. In current literature, there are several different approaches that allow us to break the diffraction limit and achieve sub wavelength imaging. The first method is near field optical microscopy (NSOM), where one relies on a NSOM probe to collect the near field evanescent wave. In the case of NSOM, the spatial resolution of near field imaging is determined by the aperture of the NSOM tip, which is typically around 50-100 nm [84]. The second method, proposed by Pendry, is based on negative refractive indexed materials, which can amplify evanescent waves and therefore achieve a higher imaging resolution [85]. However, due to the loss associated with the construction of negative index materials, sub-wavelength focusing in the optical range has yet to be demonstrated. The third approach, which is closely related to NSOM microscopy, uses various active materials at the end of the near field probe to detect the distribution of near field. In current literature, many different types of fluorescent near field probes have been developed, which can contain active materials such as semiconductor quantum dots (QDs), magneto-fluorescent nanoparticles, [86] polymer conjugates, [87] nano-complexes, and gold nanoparticles (AuNPs). [88] In all these fluorescence materials, quantum dots have some unique advantages: they have high quantum yields, broad absorption spectrum, outstanding photo-stability, and possess a tunable emission spectrum (by varying QD sizes) [89-91]. In 2003, Shubeita *et. al*. demonstrated a fluorescence resonance energy transfer experiment [92], where they used CdSe QDs as excitation donors and achieved an imaging resolution of 170 nm. The main drawback of their approach is that they could not fully control the aggregation of CdSe nanoparticles on the tip of the NSOM probe in their experiments. In 2006, Aigouy's group reported NSOM fluorescence imaging based on a tungsten tip and a 200nm silica sphere covered with CdSe quantum dots. [93]. A significant drawback of their approach is the presence

of the tungsten tip, which, being metallic, can significantly disturb the distribution of optical near field. This drawback (i.e., the usage of metallic tips) is common to almost all apertureless NSOM experiments reported in the literature.

In our project, we propose to develop a fluorescent nanoprobe based on a single carbon nanotube (CNT). The proposed nanoprobe structure is illustrated in Fig. 2-1: a single quantum dot is attached to a single carbon nanotube, which is then glued to an etched silica fiber taper tip. Our proposed nanoprobe can overcome many difficulties associated with current NSOM probes. First of all, the diameter of the CNT can be as small as 3 nm. Such a small diameter can completely eliminate any perturbation of the optical near field. The resolution of near field imaging is determined by the size of the fluorescent element, which, for a single quantum dot, can be as small as 3 nm. For applications that do not pose such a stringent requirement on spatial resolution, the attached fluorescent element can be a nanosphere covered with multiple quantum dots instead of a single quantum dot. Additionally, the CNT-based nanoprobe contains active elements and can achieve imaging functionalities that would be otherwise impossible. A few examples are the imaging of optical vacuum field and nanoscale characterization of ultrafast optical pulses. Currently, we have successfully fabricated a prototype of the nanoprobe in Fig. 2-1. Our prototype consists of an optic fiber taper, a single carbon nanotube, and silica nanospheres (100nm in diameter) covered with fluorescence quantum dots (QD@SiO_2).

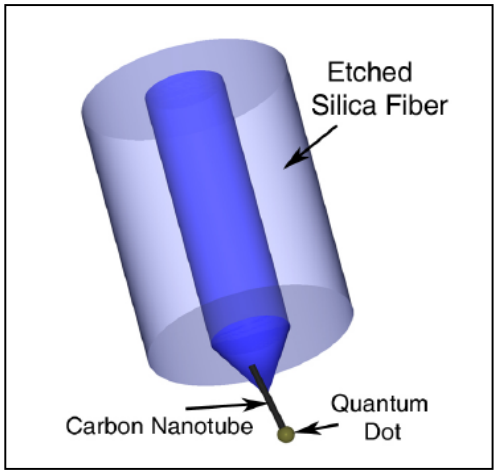

Figure 2-1. Structure scheme of a single-carbon nanotube-based fluorescent probe.

In the sections below, we provide a detailed description of the fabrication process, which includes the making of optic fiber tapers, the attachment of carbon nanotubes, the chemical synthesis of QD@SiO_2 core/shell structure, and attachment of this core/shell fluorophore to the CNT tip.

2.2 Optic fiber taper manufacturing

We have implemented two different methods to make optic fiber tapers. The first approach relies on the etching of silica fiber by hydrofluoride (HF) acid. The second method is flame- or arc-assisted taper pulling. All fibers used in our experiment are the Corning standard single mode fiber (SMF-28) with cladding diameter of 125.0 +/- 0.7um and a core diameter of 8.3 um.

2.1.1 HF etching

Hydrofluoric acid (HF) etching is a widely used in the etching of silica glass. Renato et. al. [94] has demonstrated a method of tube HF etching and has produced optic fiber tapers with a diameter of 300 nm. The main problem associated with HF etching is the sensitivity of the tip shape to environmental factors such as vibrations and temperature drifts during the etching process, which can result in rough glass surfaces.

In our experiment, the etching was carried out in a polyethylene (PE) vessel, sealed with Para film in a hood, 49.9% (v/v) HF acid and diluted 25% (v/v) HF acid were used to make fiber tapers with desired shapes. The etching device is shown below in Figure 2-2. The etching mechanism is similar to the tube etching in Ref. [94], but both the fiber end facet and its side wall are etched by HF acid. We first use the 49.9% HF acid and etch the silica fiber for 10 minutes, which is followed by etching in diluted HF acid (25% v/v). The etching rate of the 49.9% HF acid is very fast (6 um/min as reported in Otsuki's paper [95]). By using the dilute HF acid etching, we can gain much better control over the size and shape of the final silica fiber taper.

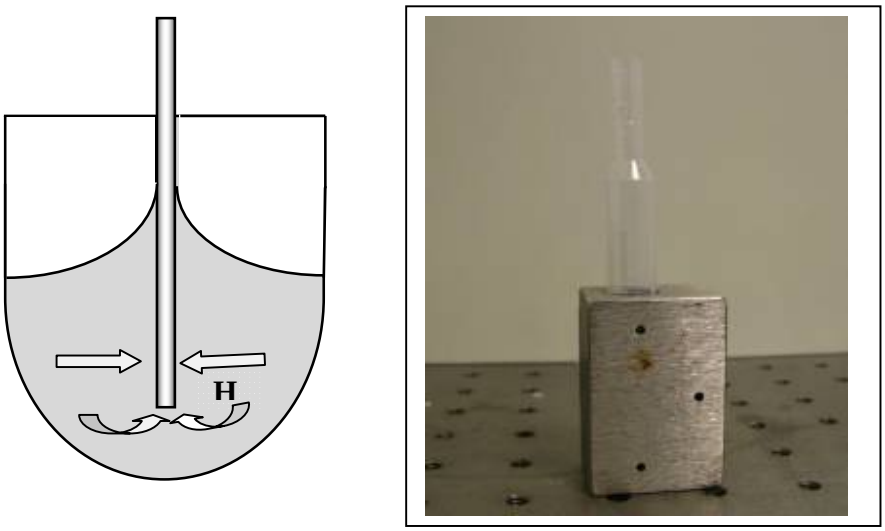

Figure 2-2. (Left) Schematic of the HF etching mechanism in the PE vessel; (Right) the etching PE vessel.

Below is the optic microscope [Zeiss Axiovert 25] image of the etched optic fiber taper. The image is taken with 10x magnification objective lens.

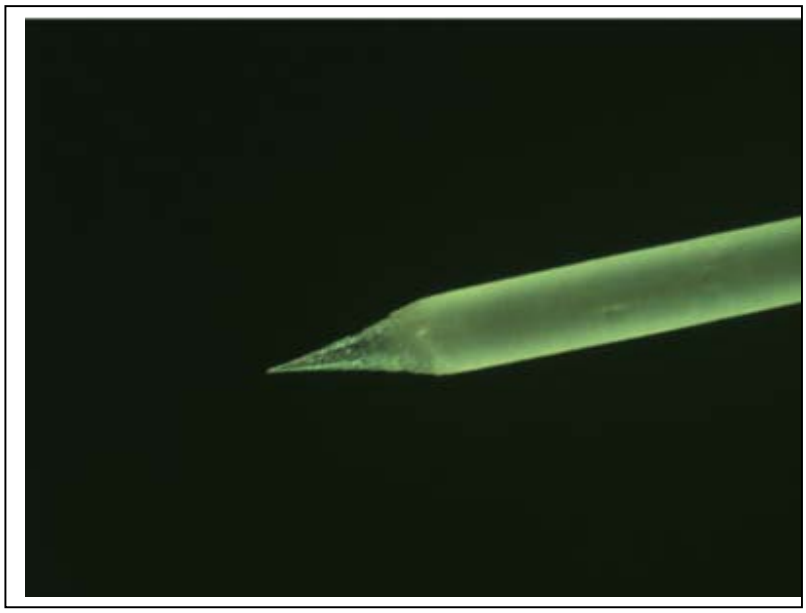

Figure 2-3. Optic microscope image of fiber taper after HF etching

In Figure 2-3, we can clearly see the surface roughness of the fiber after HF etching, as mentioned in Ref. [94]. To solve the surface roughness problem, we use different fiber pulling techniques based on heat flame, electric arc, and CO_2 laser, respectively.

2.1.2 **Flame Pulling**

Flame-assisted fiber taper pulling is commonly used for making uniform fiber tapers. Through a two step pulling process, Mazur *et. al*. has produced nanoscale fiber tapers. For the purpose of fabricating fluorescent nanoprobes, we do not require a nanoscale taper size. In our flame pulling experiments, it is sufficient to use a propane and oxygen mixture to generate high temperature. The flame pulling setup in our lab is shown in Figure 2-4.

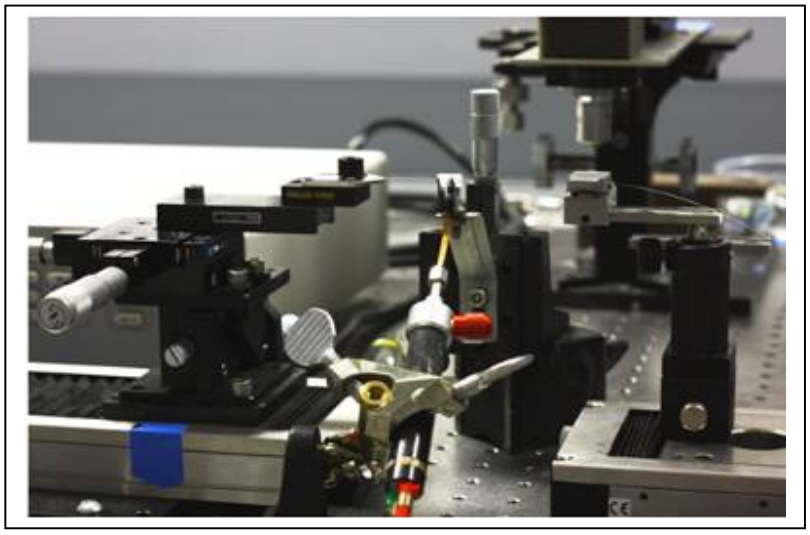

Figure 2-4: Lab image for flame pulling process to make fiber tapers.

With flame pulling, we can make fiber tapers with a uniform diameter of 3-4 microns

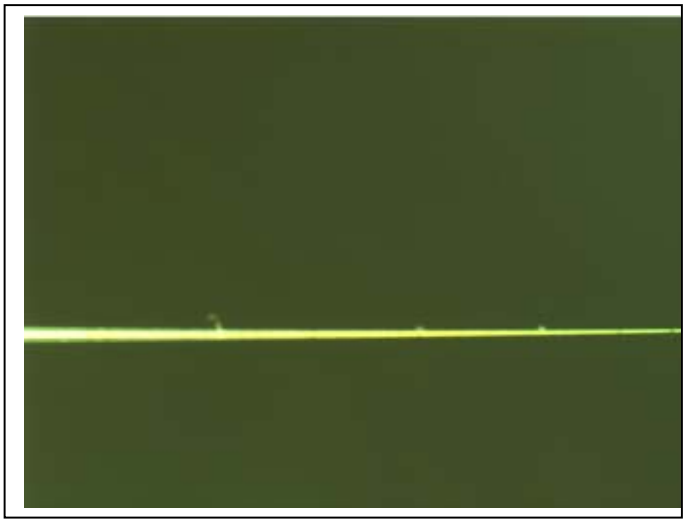

Figure 2-5. 10X magnification image of a fiber taper made by flame pulling.

A major drawback of the flame pulling technique is that the resultant fiber tapers tend to be long and easy to bend. A typical optical microscope image of the fiber taper made through flame pulling is shown in Figure 2-5. To make fiber tapers with shorter length and sharper transition profile, we can utilize the methods of electric-arc-assisted and laser-assisted pulling.

2.1.3 **Electric Arc Discharge Pulling**

The electric arc pulling was performed on Ericsson FSU-975 Fusion Splicer (see Fig 2-6), which has an auto taper pulling function. With appropriate selection of electric arc discharging time interval and intensity, this splicer can be used to make a batch of tapers in short time.

Figure 2-6. Ericsson FSU-975 Fusion Splicer

The advantage of using splicer to pull taper is that the taper fabrication process is repeatable and consistent. In contrast, tapers produced through HF etching and flame pulling tend to exhibit significant variations in taper length and shape. Since the electric arc discharge is spatially localized, the fiber taper fabricated by this technique possess a sharp transition and a short taper length. In Fig. 2-7, we show the images of the fiber taper produced by electric arc on Ericsson FSU-975 Fusion Splicer.

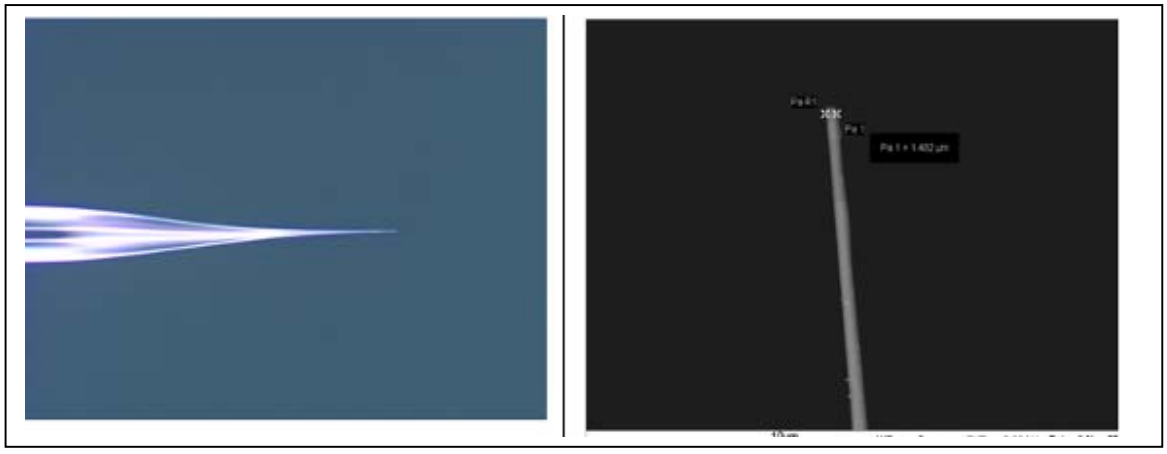

Figure 2-7. Image of fiber taper made by electric arc discharging: (Left) 10X magnification optic microscope image; (Right) FESEM image of the taper.

The diameter of the taper tip is around 1-2 μm and the length of the taper is more than 60 μm. Such a sharp taper is sturdy and not easy to bend, which is good for nanoprobe fabrication.

2.1.4 **Laser Pulling**

In laser-assisted pulling, we use CO_2 laser to heat the optic fiber, soften it, and then mechanically pull the fiber to make tapers. The pulling steps are: first, we mount the silica fiber on the linear translation stages. Then we focus the CO_2 laser on the fiber. After heating for 30s, we start the translation stage and pull the fiber until it breaks. Figure 2-8 shows optic microscopy images of the fiber tapers fabricated in our laboratory.

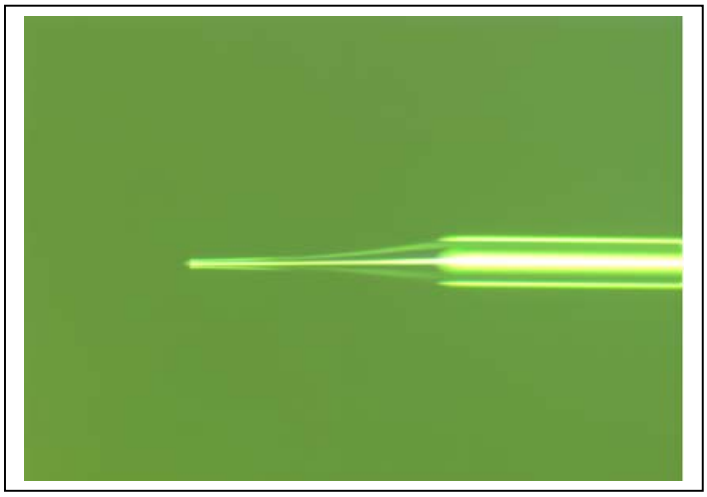

Figure 2-8. 10X magnification of the fiber taper made by laser pulling.

As we can see in lasing pulling method, the diameter of the fiber taper is around 5 um with the fiber taper pulled by fusion splicer, which was measured by FESEM to get the diameter. Since the CO2 laser is well focused on the silica fiber during the pulling process, the resultant fiber taper tends to exhibit a sharp transition and a shorter length. Also, since the pulling process is carried out in open environments, the shape of the fiber taper can exhibit some degree of variations.

2.1.5 **HF etching after pulling**

We have also developed a hybrid approach that combines the method of flame heating or electric arc and the method HF acid etching to produce high quality silica fiber tapers. In this approach, we first use a fusion splicer or flame pulling to pull a fiber with several microns in tip diameter. Then, we insert the fiber taper into HF acid (25%) vessel for 1-5 minutes. Using this method, we can fabricate submicron fiber taper while maintaining a smooth taper surface. The image of the fiber taper made through this hybrid technique is shown in Figure 2-9. Figure 2-10 shows that the taper made by this method can possess a taper diameter as small as 50 nm.

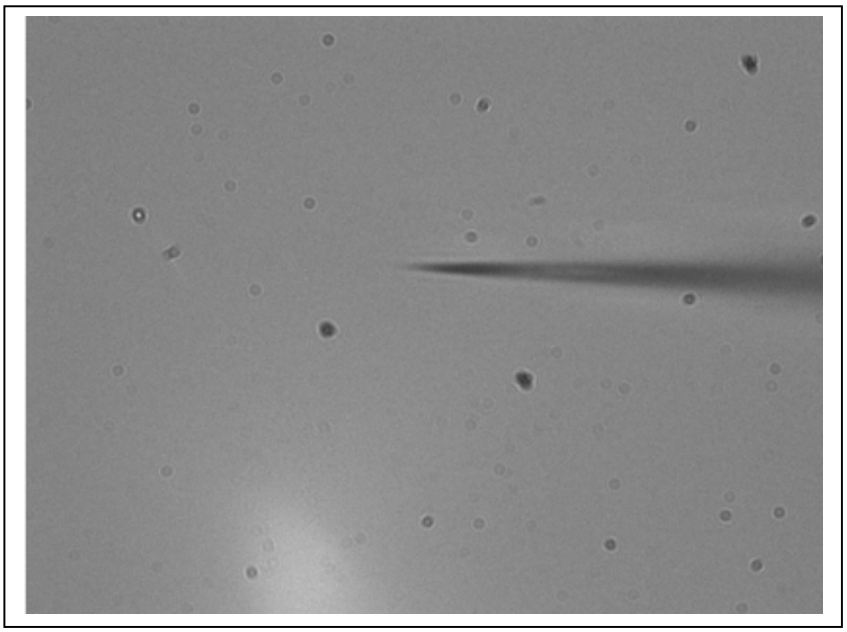

Figure 2-9. Image for a fiber taper with diameter around 50nm at our home made microscope.

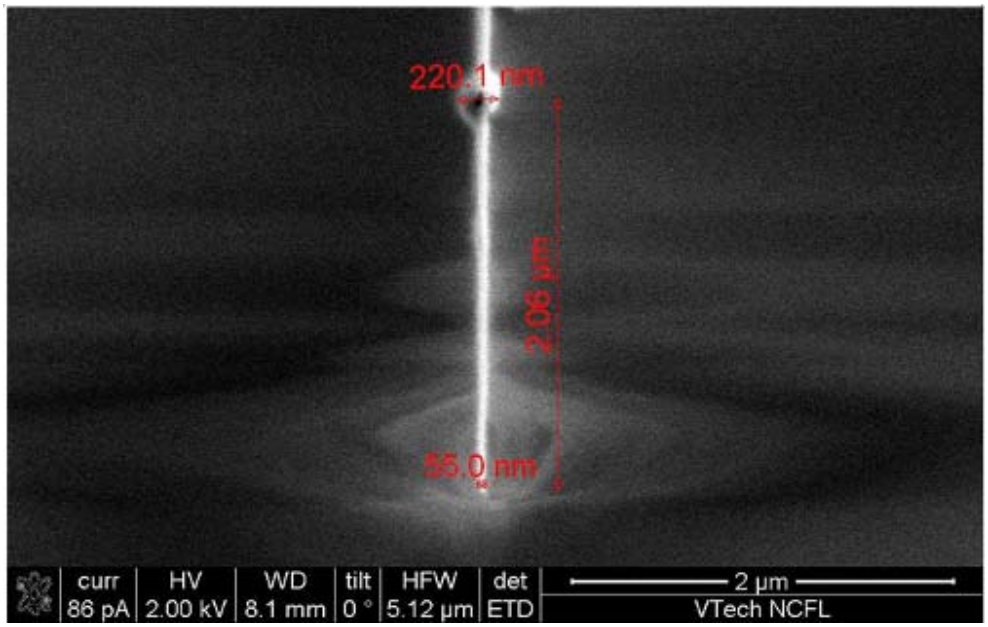

Figure 2-10. ESEM (Environmental Scanning Electronic Microscope) image for a fiber taper with diameter around 50nm.

Ren's group reported a method to 50 to 100nm diameter fiber taper with good repeatability by using the similar method. [96]. They used the fusion splicer to make micrometer long taper first and then used the HF acid (40%) to etch the taper further down to 50nm. But, their problem is that the taper angle is small, which is approximately 15 °. This decreased the light reaching the probe of the fiber. That's the same problem we had in our experiment. But we use this fiber taper just as a cantilever beam to support the carbon nanotube.

2.3 QD/SiO_2 core shell structure synthesis

Since the spatial resolution of nanoprobe imaging is determined by the size of the fluorescent element, it is important to choose an emitter with a size as small as possible. Quantum dots, organic dyes, and single fluorescent atoms all fit this requirement. However, among these fluorescent element, quantum dots have the brightest, most stable fluorescence and commercially available. Organic dyes can be easily photo-bleached while atomic emission occurs at specific wavelengths and is not easily adjustable. There are QDs available that cover a broad wavelength range from the visible to near infrared

range. The emission wavelength can be further tuned by changing the size of the quantum dot. Colloidal quantum dots are also bright and not easily bleached. They possess high quantum efficiency and can generate stimulated emission [97].

Since the size of quantum dot is only 4-5 nm, which is far beyond the resolving capability of an optical microscope, it is difficult to manipulate a single quantum dot under an optical microscope. We have two ways to solve this issue: the first one is to use an alternative method in which we attach quantum dots to the bigger sized silica nanosphere, then use these silica nanospheres as fluorescence elements instead of directly attaching quantum dots. The second method is to use a chemical reaction to covalently bond quantum dots to the end of a carbon nanotube. Both methods allow us to manipulate fluorescent elements through optical microscopy.

In the first method, we use silica nanospheres coated with multiple quantum dots as the fluorescence element. One advantage of this approach is that, with multiple quantum dots, the fluorescent signal from the light emitting element can be significantly enhanced, which is particularly important for infrared quantum dots. In addition, by using nanospheres with diameter in the range of 100 nm, it is possible for us to pick up these nanospheres under an optical microscope.

The coating process is similar to the method reported by Langbein *et. al*., in Ref. [98]. The quantum dots we used in our experiment are obtained commercially from Evident Technology. The QDs possess a CdSe/ZnS core shell structure with 4.3nm in diameter. The central emission peak of the QDs is at 610nm. The silica nanospheres (100 nm diameter) are bought from Polyscience Inc, in colloidal form. To cover the surface of the nanospheres with QDs, we first heat the toluene to 80 °C, and then add 3% solution of (3-mercaptopropyl) trimethoxysilane (MPTS) for 1% v/v to the toluene. We subsequently add, drop by drop, the solution containing silica nanospheres under vertex mixing. After the silica colloid solution has been dissolved into the toluene, we add a few drops of CdSe/ZnS quantum dot. Let the reaction proceed for another 5 minutes then use ultrahigh speed centrifuge to wash the products with toluene for 4-5 folds

The basic principle of the reaction was drawn in below:

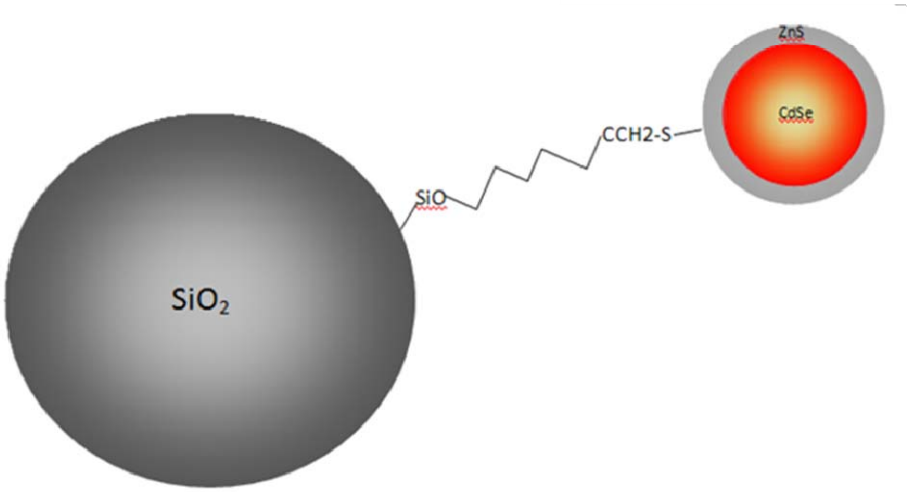

Figure 2-11. Scheme for prepare CdSe/ZnS onto the SiO_2 surface to form core/shell nanosphere via chemical synthesize

This reaction would produce a near monolayer of MPTS on the surface of the silica nanospheres. Then the spheres with the MPTS-activated surface were mixed with a highly diluted colloidal solution of CdSe@ZnS quantum dots in toluene. Under stirring, the CdSe@ZnS dots are bounded to the surface of nanospheres via formation of S-Zn ligand between surface Zn atoms and MPTS mercapto groups.

To verify that QDs were successfully attached to the surface of SiO_2 nanosphere, we used the TEM (Philips EM 420 Scanning Transmission Electron Microscope) to characterize the final product. As show in figure 2-12(left), which is the TEM image for the SiO_2 nanosphere before coating; and the figure 2-12 (right) is the TEM image for the SiO_2 after coating with the CdSe/ZnS core shell quantum dots. As we could see in figure 2-12 (right), around 10-20 quantum dots were attached to the SiO_2 surface.

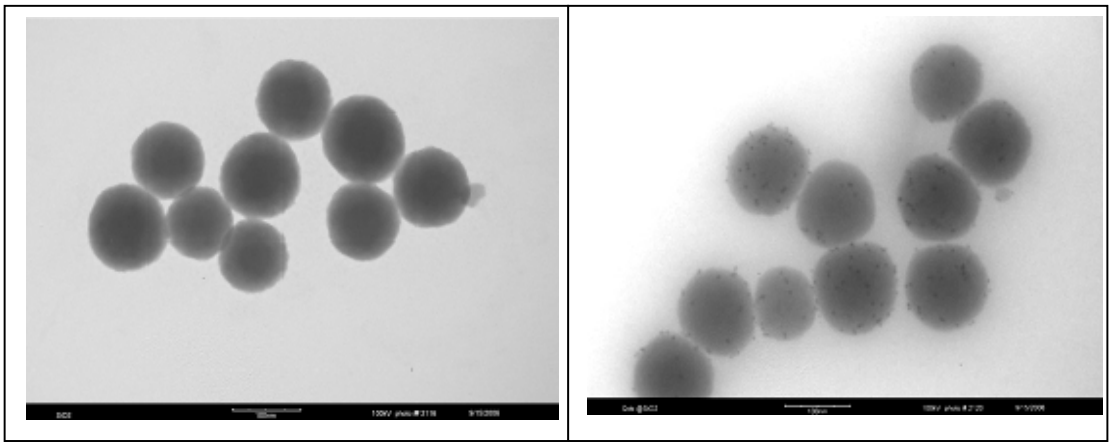

Figure 2-12. FESEM images for SiO_2 and CdSe/ZnS@SiO_2 core shell nanospheres: (Left) SiO_2 nanospheres before synthesis reaction; (Right) CdSe/ZnS@SiO_2 core shell nanospheres after reaction

2.4 Carbon nanotube surface modification

In our design, we mainly use carbon nanotubes for the purpose of non-perturbative near field imaging. From electromagnetic theory, we know that for a small sphere with a volume V and a dielectric constant ε_r, the total scattering cross-section σ is given by Equation (2) [99]:

$$\sigma = \frac{3}{2\pi} k^4 V^2 \left| \frac{\varepsilon_r - 1}{\varepsilon_r + 2} \right|^2 \qquad (2)$$

where *k* is the wave vector in air. This suggests that for a thin dielectric cylinder with diameter *d*, the optical scattering induced by the cylinder should decrease as d^4 (since $V \sim d^2$). Let us first consider a state of the art dielectric probe with tip diameter 125 nm [100], and a carbon nanotube probe with a diameter of 10 nm. From above equation, we concluded that the scattering induced by a carbon nanotube can be four orders of magnitude smaller than the state of the art dielectric probe. The dielectric probe [101] can

produces a wavelength shift of the order of 10 nm; yet the corresponding wavelength shift induced by a 10 nm diameter nanotube should be less than 10^{-3} nm, which is sufficiently small for most high Q cavity applications.

2.5 Quantum Dots Covalent bonding to CNTs

The ends of the carbon nanotubes are more metallic than the side walls, due to the concentration of pentagonal defects [102]. These defects also cause the high activity of tube ends, which make it easier to have chemical reaction at the end of the CNTs. It has been reported to open the carbon nanotubes [103] by chemical treatment in strong acid at high temperature [104], or filling the tubes with foreign substances, like drugs in the medical application in drug delivery [105-107].

Functionalized nanotubes were used with AFM tips to perform measurement about the binding forces between protein-ligand pairs and imaging chemically patterned substrates. The chemical modification of nanotubes is a major issue with far-reaching implications. The possibility to manipulate, chemically modify and perhaps polymerize nanotubes in solution will set the stage for nanotube-based molecular engineering and many new nano technological applications [108].

Several chemical processes have been developed to directly attach quantum dots to both ends of a single carbon nanotube [109, 110]. The principal synthesis procedures include majorly three steps.

The first step is to use chemicals to clean the CNT via chemicals for future covalent bonding reaction. The tips of MWCNTs, which have the highest defect sites, get oxidized first.

The detail of this step is: first, add 0.1g CNTs to the three-neck round bottle flask, then filled the flask to 1/3 with HNO_3, then reflux the mixture at 118 °C for 24 hours. After cooled to room temperature, di-water was used to wash the mixture with repeated centrifuge till the solution PH value reach 6-8. This step removed and cleans amorphous

carbon from CNTs and opened the active region on both end of the CNT and created a carboxylic group that terminated the CNT end.

The figure in below shows the TEM image of Carbon nanotube before and after chemical cleaning. In figure 2-13(left), we could find amorphous carbon on the side wall of the CNT. After chemical cleaning, in figure 2-13(right), we could find that the amorphous carbon disappeared, though there was still little amorphous carbon left at the end of the carbon nanotube.

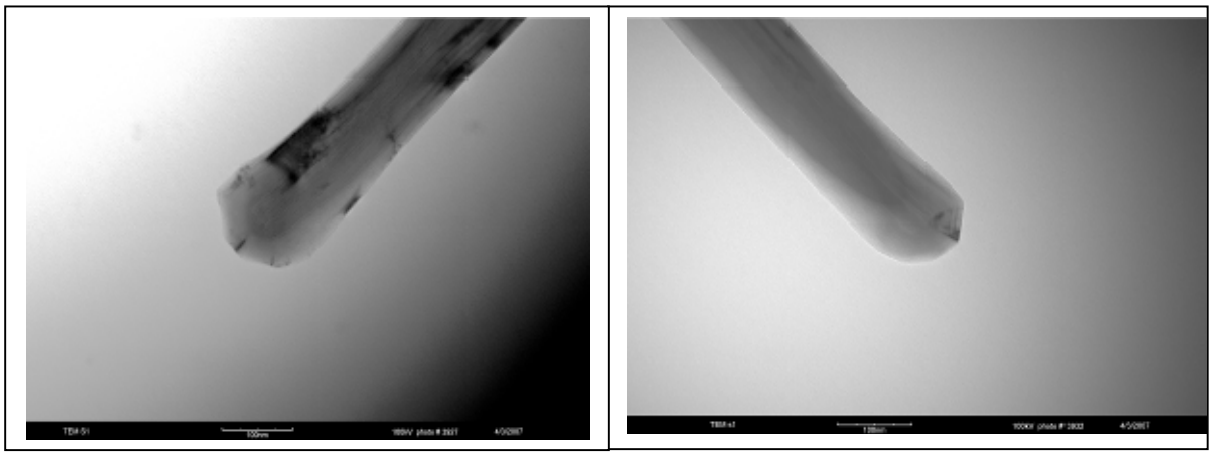

Figure 2-13. TEM images for carbon nanotube we used in our nanoprobe fabrication: (Left) before chemical cleaning; (Right) after chemical cleaning in HNO_3 reflex at 118 °C for 24 hours.

The acid-treated CNTs were washed with di-water several times and vacuum filtered using a 0.1-*u*m polycarbonate filter. The acid treatment introduced acid groups at the end of the CNT; also the oxidation removed the graphitic amorphous carbon away from CNTs. After oxidation, the CNTs were shorter and were left with the carboxylic groups that imparted a hydrophilic nature and facilitate further modification [111].

Next we functionalized ZnS capped CdSe quantum dots by agitating with 2-aminoethane thiol hydrochloride (AET) in aqueous solution.

To prepare water stabilized QDs (QD-NH2), ZnS-capped CdSe nanocrystals were suspended in chloroform by sonication for 30 min. Equal volumes of 1.0 M 2-aminoethane thiol hydrochloride (AET) were added to this QD solution. This resulted in a two-phase mixture with the aqueous aminoethane thiol forming an immiscible layer above the organic chloroform- QD suspension. The mixture was stirred vigorously on a magnetic plate for 4 h, after which it was allowed to settle down for a few minutes. Phosphate buffer saline (PBS, pH7.5) was added to the solution in a 1:1 volume ratio. This was then mixed again in a vortex mixer for 1 h. The water stabilized QDs were separated from AET by centrifuging the solution and re-suspending them in PBS a couple of times [111]. When ZnS-capped CdSe QDs were reacted with AET, the mercapto group in the thiol bonded to the Zn atoms, and the amine groups rendered the QDs hydrophilic, in addition to facilitating further modification possibilities.

Finally, we mixed the carbon nanotubes and the quantum dots together, which linked quantum dots to both ends of the nanotube through covalent coupling. After obtaining carbon nanotubes with both ends attached to quantum dots, we focus a high intensity laser beam on the center of the nanotube and cut it in half. In the future, we can ensure only a single quantum dot is attached to one end of the nanotube through photon anti-bunching measurements. Finally, we can glue this nanotube, which possesses a single quantum dot to etched silica taper. This gave us the single quantum dot probe shown in figure 2-1. The details of the CNT-QD heterostructures formation was a two-step coupling procedure using 1-ethyl-3-(3-dimethylaminopropyl) carbodiimide HCl (EDC, Pierce Chemicals, Inc.) in the presence of *N*-hydroxysuccinimide (sulfo-NHS, Pierce Chemicals, Inc.), and the reaction was carried out in PBS. Here, the EDC reagent activated the terminal carboxylic groups of the CNTs forming a highly reactive o-acylisourea intermediate, which underwent a rapid hydrolysis to form the acid again. However, in the presence of sulfo-NHS, a more water soluble sulfo-succinimidyl intermediate was formed. This intermediate readily underwent nucleophilic substitution with primary amines on the QD surface, forming amide linkages. The EDC reaction was carried out for 8 h at 50 °C under continuous mixing.

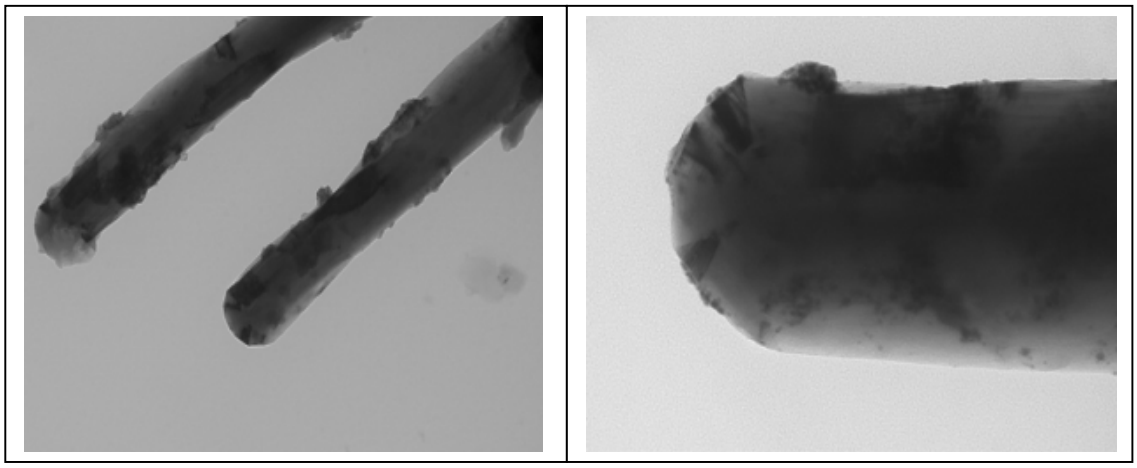

Figure 2-14. TEM image of the MWCNT covalent bonded with quantum dots at side walls and heads of MWCNT.

Figure 2-14 showed the TEM image of the MWCNT covalent coupling with QDs without chemical cleaning process, in which we could find that both side walls and end of CNTs were connected with QDs. The following figures, figure 2-15 (left) and figure 2-15 (right), are the figure for the CNT covalent bonded with QDs, in which CNT was refluxed in HNO_3 for 24 hours. The chemical acid refluxing of CNT in acid removed the amorphous carbons on the wall of CNT and opened the active region on the end of the CNT and creates a carboxylic group that terminates the CNT end. Because there are more defects and active region in these end area, it is easier being attacked by water solvable QDs.

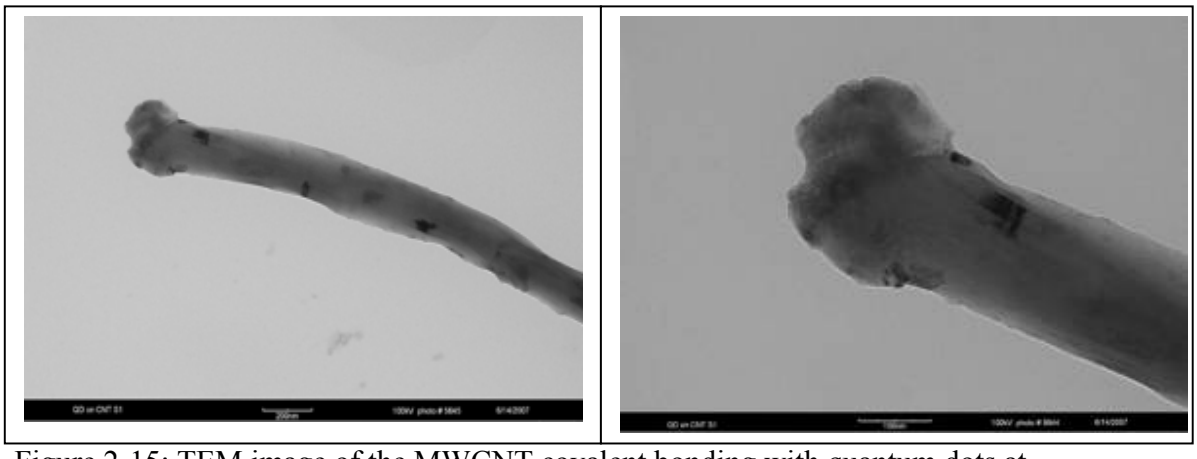

Figure 2-15: TEM image of the MWCNT covalent bonding with quantum dots at selective position of the end of MWCNT.

As we can see in the above figure, most of the QDs aggregated at the end of the CNT, which is the desired position.

2.6 Nanoprobe fabrication: QD@SiO_2 at the tip of CNT

After we synthesized the QDs@SiO_2 core shell nanostructures, MWCNT covalent bonded with QDs at the end, and fiber taper, we are ready for the fabrication of the fluorescence nanoprobe. We can proceed with two different approaches. The first one is to use UV glue to attach a single MWCNT to the end of the taper. Then use this nanoprobe to pick the fluorescence element, QDs@SiO_2 core shell nanostructure. The fluorescence nanoprobe fabrication process is schematically shown below in figure 2-16.

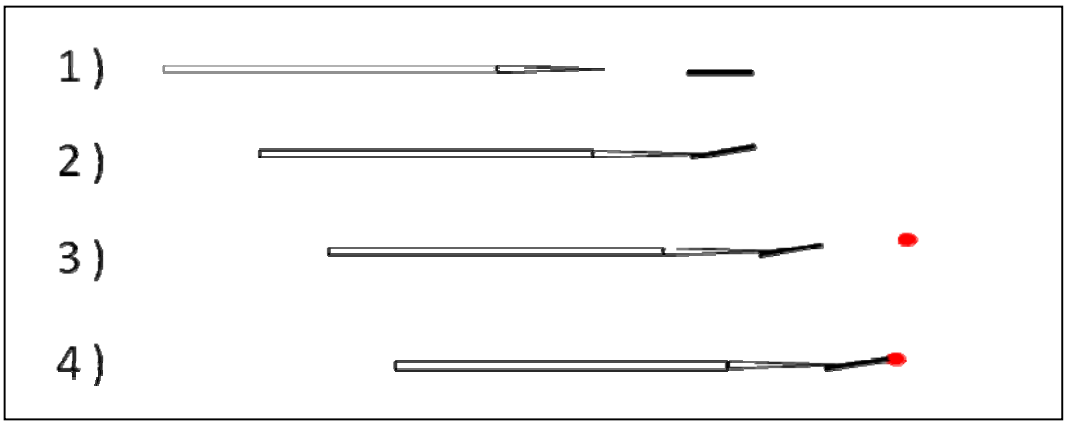

Figure 2-16. Scheme for the fluorescence nanoprobe fabrication processes: (1) locate fiber taper and MWCNT in the view range of our home made microscope; (2) move the taper to pick up one single MWCNT and solidified with UV glue after UV curing; (3) use fluorescence microscope image to locate the position of fluorescent elements; (4) use the taper with single MWCNT to pick up CdSe@ZnS @SiO_2 fluorescent nanospheres.

Second method is to use the MWCNT covalently bonded with QDs and then use fiber taper to pick one of these MWCNT as fluorescence nanoprobe.

2.6.1 Attach Single Carbon nanotube to fiber taper

Here is the really time CCD images we grabbed during the fluorescence nanoprobe fabrication. The figure 2-17 (left) is the image of the optic fiber taper and single MWCNT before attachment. Second image in figure 2-17(right) is the CCD image of the optic fiber taper glued with single MWCNT. The image was grabbed under our self-designed homemade optic microscope, which used a 20x magnification long working distance lens and Imaging Source DMK21F04 monochromator 1/4" CCD camera, which is connected with firewire.

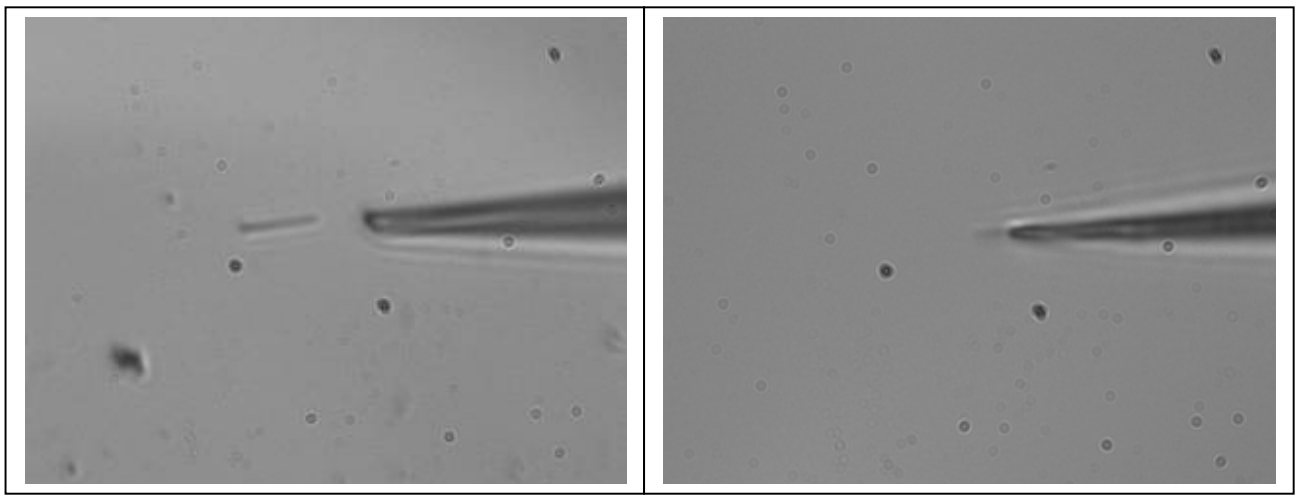

Figure 2-17. Carbon nanotube and fiber taper image on our home made microscope: (Left) single MWCNT and fiber taper before attachment; (Right) fiber taper and the single MWCNT after attachment.

Here is the FESEM image (figure 2-18)of the taper glue with a single MWCNT. The lower bump part on the fiber taper is the UV glue.

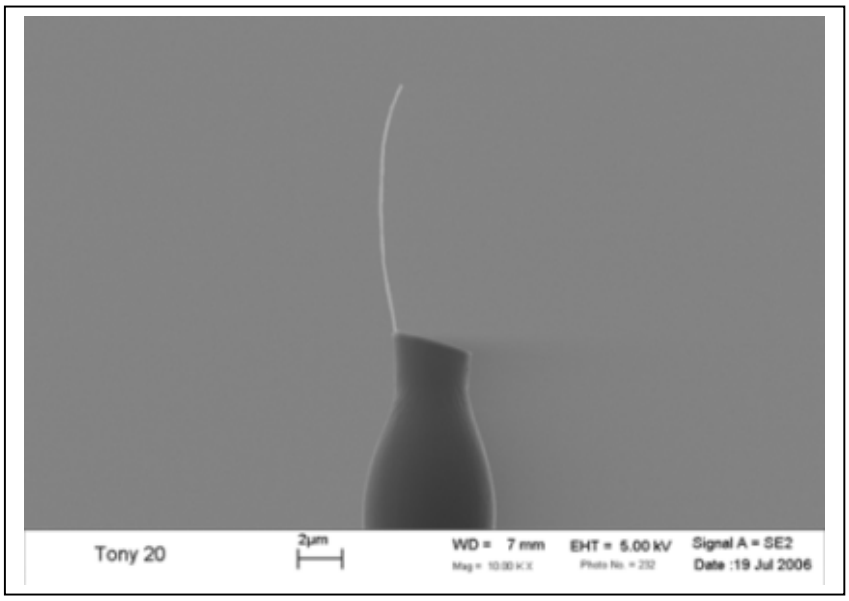

Figure 2-18. FESEM image of the fiber taper with single MWCNT.

Now we can successfully locate and pick up single CNT. If we used the QD covalently modified MWCNT, it could be served as fluoresce nanoprobe.

2.6.2 Pick-up QD@SiO_2 to the tip of CNT

To make the fluorescence nanoprobe, in the second method, we used a single bare MWCNT without QDS covalent bonding to pick up QD@SiO_2 as fluorescence element.

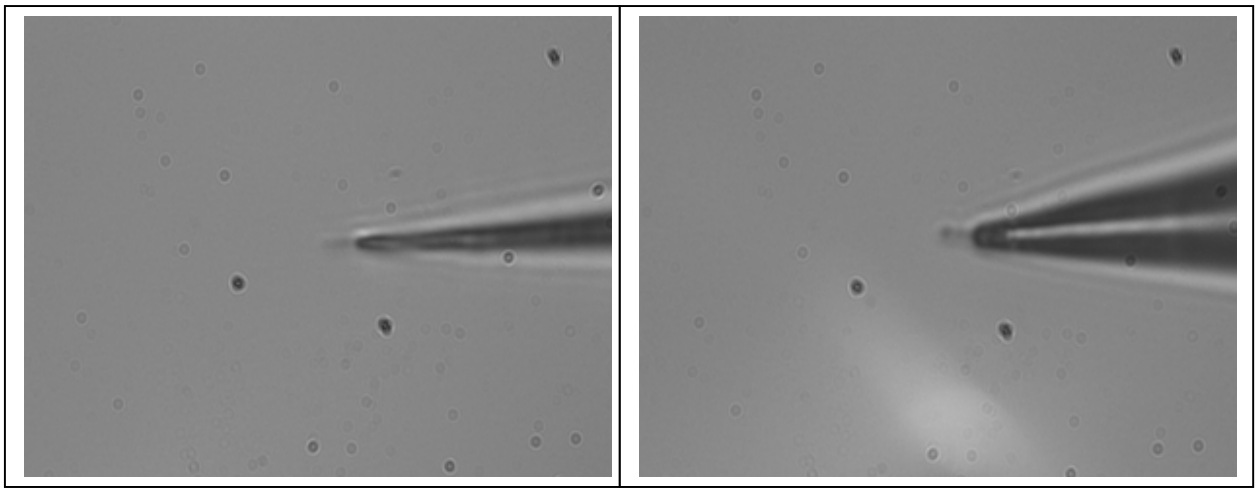
Figure 2-19. Image of the Fiber taper with single MWCNT before (Left) and after (Right) pick up the CdSe@ZnS on SiO_2 nanospheres on our home made microscope.

The above two images were the CCD images of the nanoprobe of the optic fiber taper with MWCNT before and after pick up QD@SiO_2 core shell nanospheres. The left one in figure is the image before attachment; the right one is the image showing that QD@SiO_2 attached to the end of MWCNT tip on fiber taper.

To verify the successful attachment, we used two methods to see whether it had been attached to the MWCNT tip. The first method is pretty simple. After attachment, we used a UV gun (Eletro-Lite Corp, ELC-404) to shine on the fluorescence nanoprobe. The image of the fluorescence nanoprobe was shown in below in figure 2-20 (left). From the image, we could see that it was brighter at the end of the MWCNT tip than any other parts of the nanoprobe. So it gave us a rough idea whether the fluorescence elements were attached to the nanoprobe and what the location of the elements attached to the nanoprobe. Second method is to use the FESEM to have close view of the details and nanostructure of the fluorescence nanoprobe. The FESEM image of the nanoprobe was shown in figure 2-21 (Right).

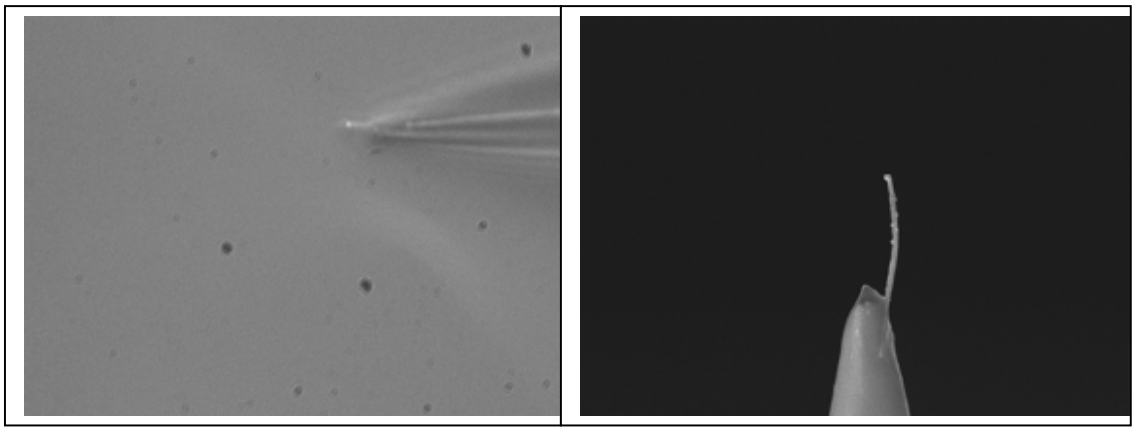

Figure 2-20. (Left) The image of the taper with single MWCNT after pick up CdSe@ZnS on SiO_2 nanospheres under UV light; (Right) FESEM image of the taper with single MWCNT after pick up CdSe@ZnS on SiO_2 nanospheres.

From figure 2-21(Right), we could see that there was something at the tip of the MWCNT. So it was consistent with the result we got from the UV gun. But there were still some bumps on the side wall of the MWCNT (figure 2-21 left). They are QDs@SiO_2

nanospheres, which were measured under FESEM. The size of these bumps was around 100nm which was the same of the SiO2 nanosphere.

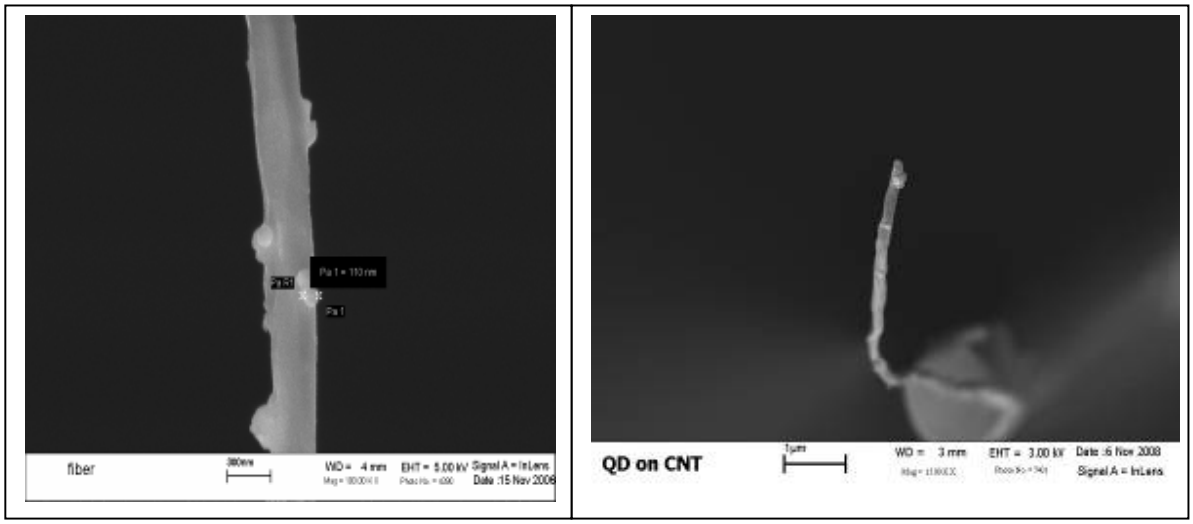

Figure 2-21. FESEM image of MWCNT with CdSe@ZnS on SiO_2 nanospheres.

But with careful manipulation and pick up, we can avoid gluing the QD@SiO_2 to the side of the MWCNT. We could purposely locate them at the end of MWCNT. The left image in Figure 2-21 (Right) is the top view of a fluorescence nanoprobe with only three QD@SiO_2 nanospheres at the end of a single MWCNT.

2.7 Conclusion

Optic fiber tapers were fabricated via HF etching, flame pulling and electric arc pulling. Different techniques make different shape and ration of the fiber taper. By using etching after pulling method, we could lower the diameter of our fiber taper to 20nm at minimum.

MWCNTs were attached to the fiber taper and quantum dots (QDs) were successfully covalent bonded to the end of MWCNTs via chemical synthesis. This was one of the routes we made our fluorescence nanoprobes. Another method was used to fabricate nanoprobe: first, quantum dots were chemically synthesized to the surface of SiO_2 to form the QD@SiO_2 core-shell structures, then used the MWCNT at fiber taper to pickup

these QD@SiO_2 to form the fluorescence nanoprobe. With careful manipulation of the nanoprobe and application of fluorescence imaging, we could control the number of QD@SiO_2 nanosphere to 3 or several, less than 10, which is first reported with clear FESEM image as evidence.

3 Nanoprobe Fabrication System and Fluorescence Scanning system

In our lab, the fluorescence scanning system is integrated with the nanoprobe fabrication part. We tried to design a system so that we could break the diffraction limit of the optic microscope to handle 100nm SiO_2 nanospheres and MWCNT which is around 147 nm in diameter and several micrometers in length.

3.1 Nanoprobe Fabrication System Design

The basic idea of the nanoprobe fabrication system came from epi- confocal microscope, where in our set-up we did modification in order to pick up QD@SiO_2 nanospheres and MWCNT. The commercially available confocal microscope has very short working distance.

In confocal microscope, the laser was focused by an objective lens to the sample of interested; while the signal from the sample was also collected by the same objective lens. Dichromatic mirror was used to bend the green laser into the objective lens, and then let the red fluorescence signal only pass though the dichromatic mirror. The dichromatic mirror worked as a filter and beam splitter.

Our home made fluorescence confocal microscope was made based on the idea from epi-confocal microscope. We used a 20x magnification Mitutoyo Long working distance lens and two 3D translation stages to fabricate fluorescence nanoprobe. We dispersed the MWCNT water solution onto the glass slide, then put this glass slide onto one translation stage, then used another translation stage with optic fiber taper to pick up one of these MWCNTs and UV cued with Loctile 3105 optic adhesive. After we got the nanoprobe consisted with fiber taper and MWCNT, we used this nanoprobe to pick up the fluorescence element QD@SiO_2. Since QD@SiO_2 was only 100nm which is smaller than the diffraction limit, we used 532nm green CW laser to locate these QD@SiO_2

nanospheres first, then switched to white light to manipulate the nanoprobe. The system scheme is shown in below:

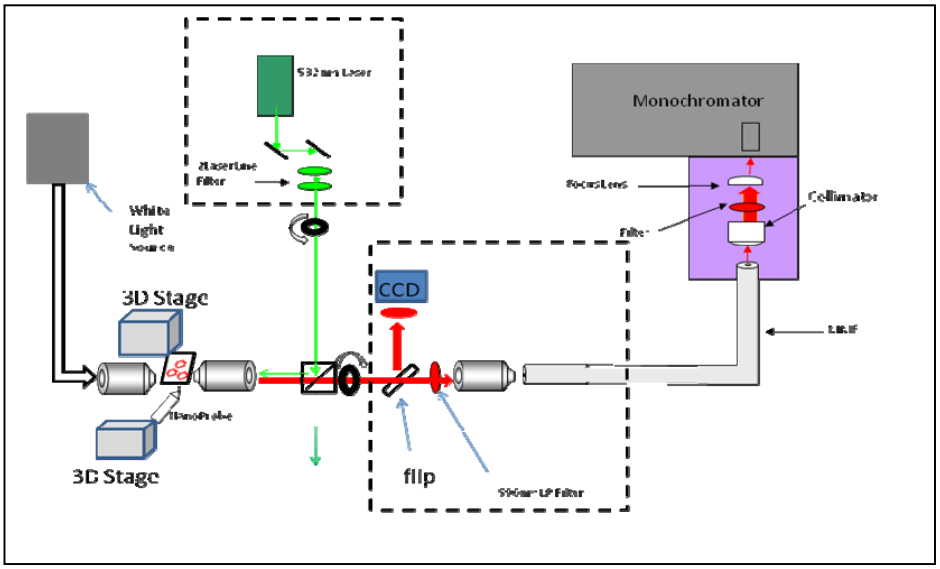

Figure 3-1. Scheme for the nanoprobe fabrication system setup.

Next figure is the lab image of the nanoprobe fabrication system, which could give us a vivid image of our system.

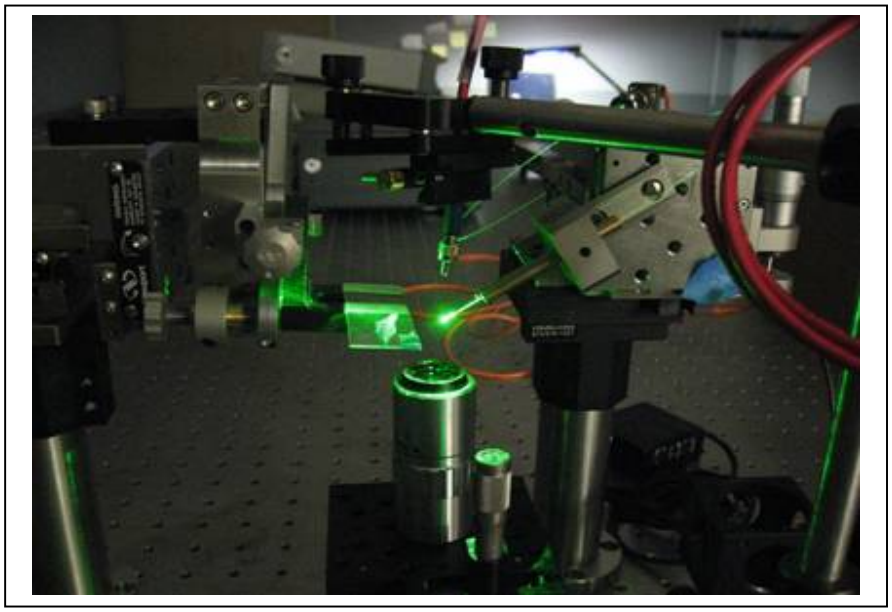

Figure 3-2. Lab image of the nanoprobe fabrication system setup.

Up to now, we have successfully fabricated fluorescence nanoprobes. Then the next step is to use this nanoprobe to do fluorescence scanning to image nanostructures.

3.2 Fluorescence Scanning System

In order to demonstrate the application and abilities of our fluorescence nanoprobe, we added one piezoelectric stage to do the scanning. The piezo stage was PI P611.3S nanocube system, which consisted of a piezoelectric stage with 1 nm resolution, a controller and serve module for amplifier. The monochromator could be replaced by PMT for fast scanning, and CCD camera was also used to record the fluorescence images when the nanoprobe was under scanning.

The next figure is the scheme we used to do the fluorescence scanning near the focus area of the objective lens. This scanning could tell us the intensity information of the focus area from point to pint, which was usually only being studied for the average intensity or the size of the focus area. Our nanoprobe could tell us more about this area.

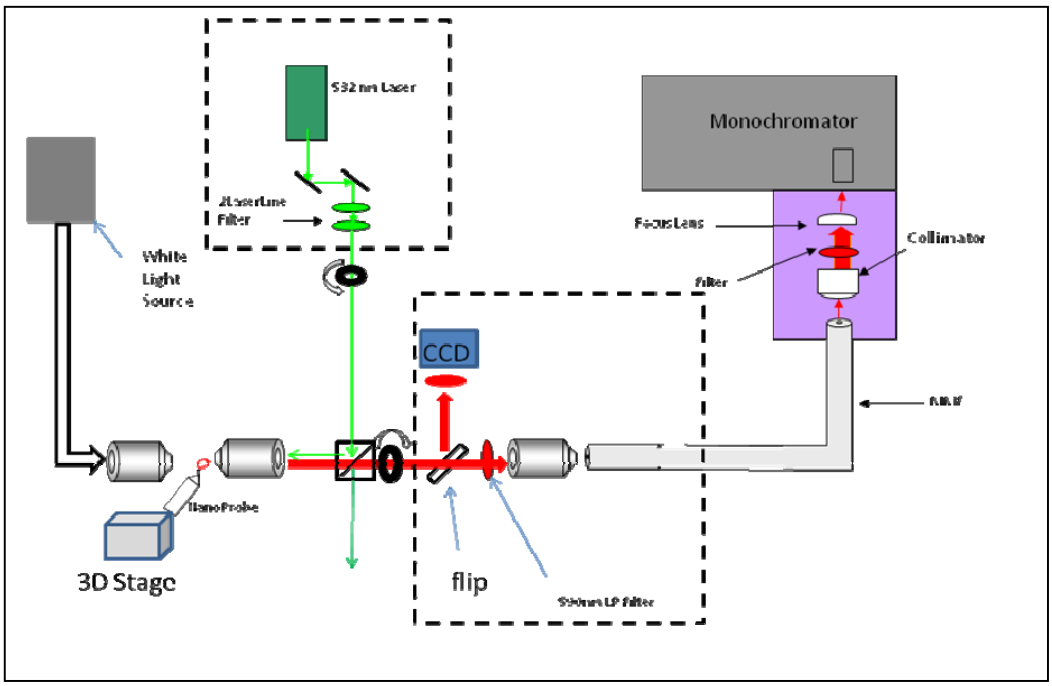

Figure 3-3. Scheme for fluorescence scanning system setup.

Here is the fluorescence image of the fluorescence nanoprobe we fabricated on our system. The left one is the image taken under white light source. In this figure, the dark rod is the optic fiber taper with diameter around 1-2 um and the curved line is the MWCNT, which is only 147 nm that below the diffraction limit so it looks not as solid as the fiber taper. The left one is the image when we lower the power of the white light source and turn on the 532 nm CW laser. This image was taken with 532 notch and 535 Long pass and 590 long pass filters. In this image, we could clearly find that the fluorescence element was put on the tip of the MWCNT.

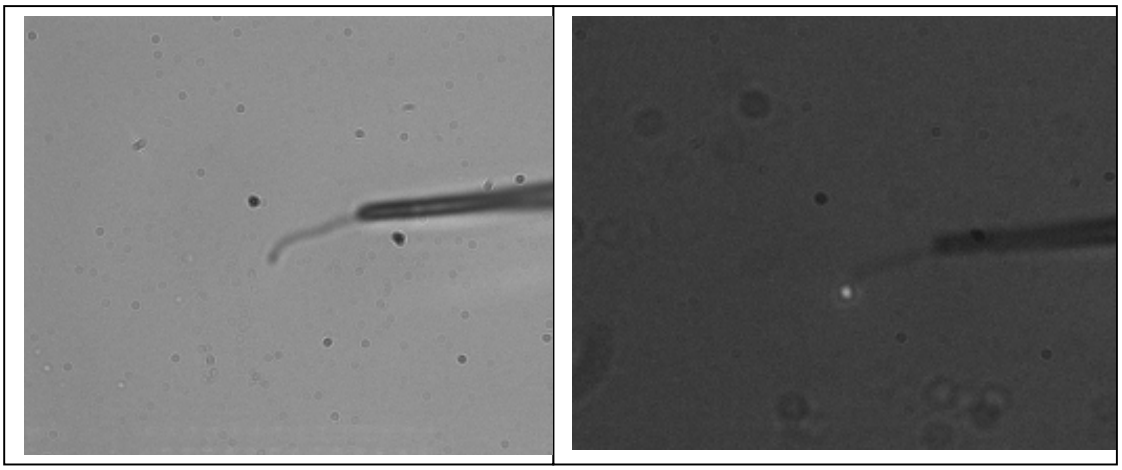

Figure 3-4. Image of the fluorescence nanoprobe: (Left) White light source image; (Right) fluorescence image with weak white light

To verify the fluorescence, we shut down the white light source, keep on only 532nm green laser, with 532 nm notch filter and 535 nm and 590 nm long pass filters. In this image, we could only see the bright spot at the same position with previous figure. The FESEM picture showed the nanostructure of this nanoprobe, which consisted of 10-20 QD@SiO_2 nanospheres.

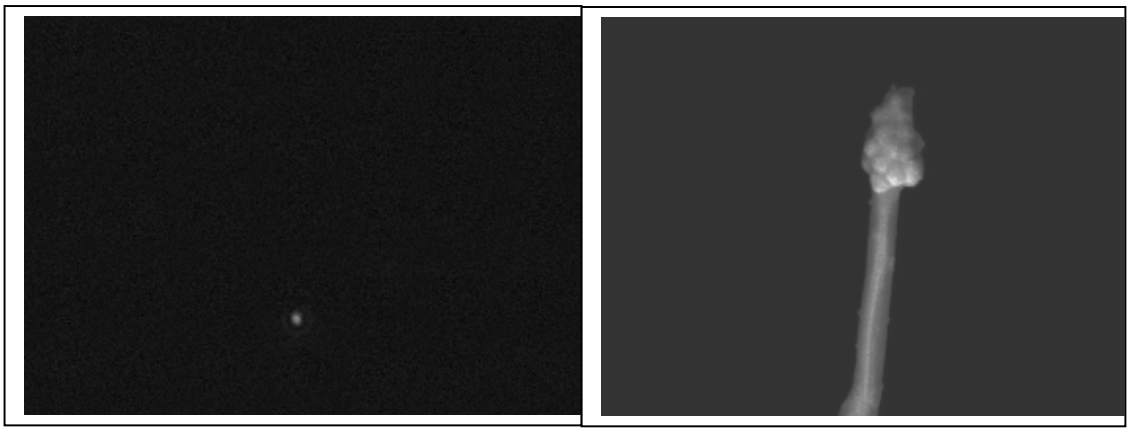

Figure 3-5. Fluorescence image of the fluorescence nanoprobe and its FESEM image.

All those images showed the successful fabrication of the fluorescence nanoprobe.

3.3 Florescence Spectrum

The spectrum measurement setup is the same as the fluorescence image collection setup in figure 3-4. Only difference on the setup is lift up the flip mount ahead of the CCD camera to let the fluorescence signal pass the flip mount and focused by a 20X magnification objective lens and coupled the signal into a SMA fiber bundle, which went to the slit of liquid nitrogen cooled monochromator (Princeton Instruments Acton SpectraPro 2500i). Here is the spectrum we got from the monochromator.

The first one is the spectrum of the back ground from environment.

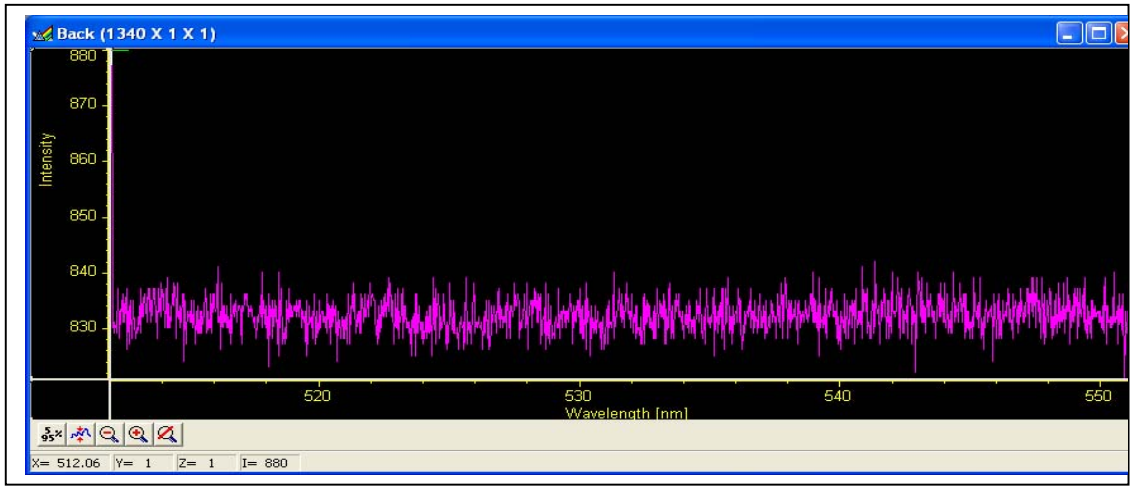

Figure 3-6. Back ground spectrum of the environment.

We took this one as the base line of future measurement. Then we insert a pure silica fiber taper, with nothing on the taper head, into the focused laser beam, collected the spectrum from this pure fiber taper. The spectrum we got is shown in below which gives us the information about the silica taper spectrum. As we can see from figure 3-8, there is no fluorescence from silica fiber taper. Back ground spectrum was automatically subtract from the spectrum of the silica fiber taper.

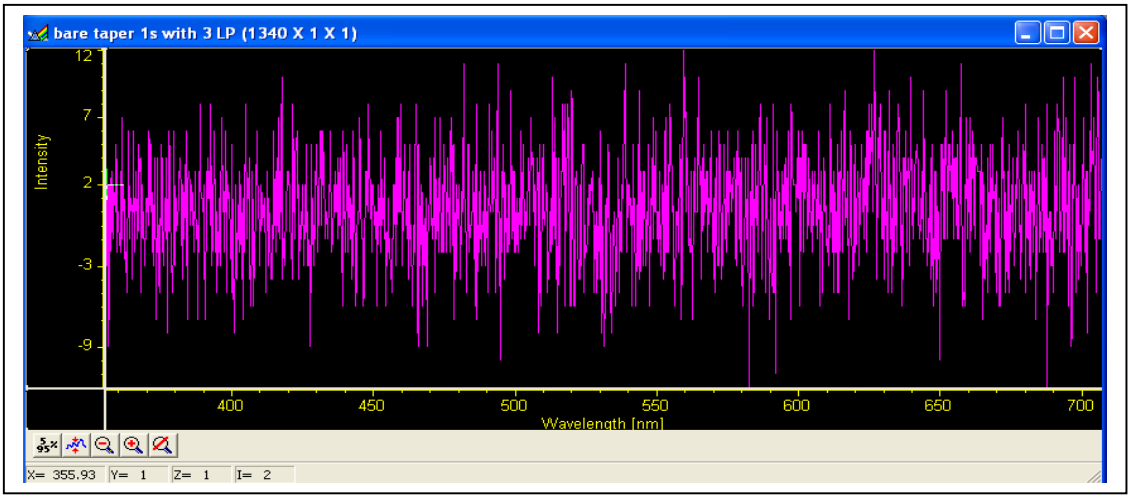

Figure 3-7. Spectrum of the bare fiber taper.

After we confirm the spectrum of the silica fiber taper, then we insert our fluorescence nanoprobe into the focus area of the laser beam and collected the spectrum from the nanoprobe. The spectrum was shown in next figure 3-9.

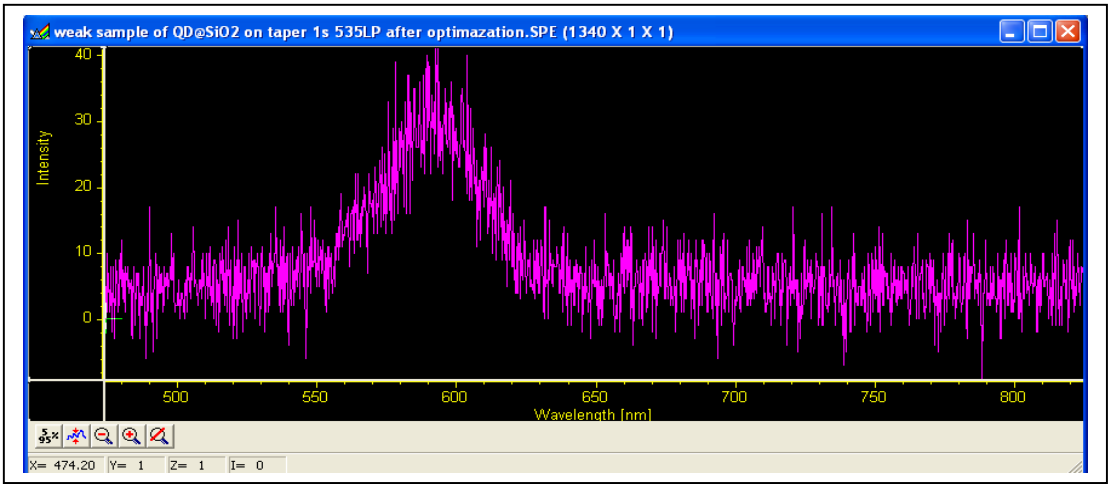

Figure 3-8. Spectrum of the fluorescence nanoprobe.

From figure 3-8 and 3-9, we could clear see the spectrum of fluorescence. It is consistent with the excitation spectrum of the quantum dots CdSe/ZnS. The spectrum of the quantum dots from company is available on line [112]. So this approved that the fluorescence image got before are the fluorescence we want which is emitted by the quantum dots.

3.4 Scanning Image of focused laser beam

This experiment was carried out to study the focused laser beam at the focus point. At present, we could measure the power of the focused laser, or study the shape of the laser, but we could not see the details about the intensity distribution of the focused laser beam. With our nanoprobe, we can use it to do the 2D or 3D scanning in the focus area of the laser beam and collected the signal of the fluorescence. By computer re-construction, we can get the intensity distribution of the focus point of the laser beam, and also the shape of the focused point. The figures in below were the result we got by scanning our nanoprobe in the focus point of laser beam.

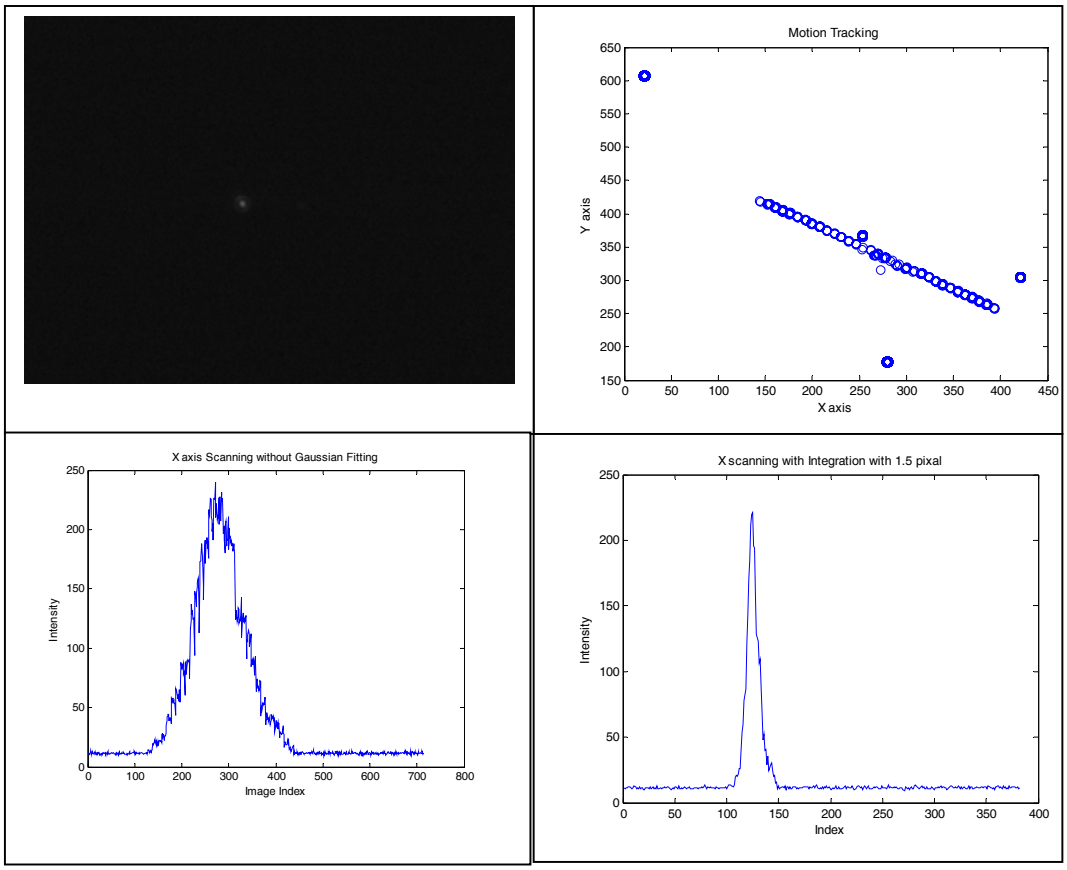

Figure 3-9. Scanning result of the focus area of the laser beam.

The first figure is the fluorescence image of the nanoprobe, in which we could only barely see a tiny white spot. It was because that only very few fluorescence element was attached to the nanoprobe. The second (upper right one) figure is the motion tracking image to find out the track of the scanning route. In this figure, we can find that the nanoprobe scanning is straight with only few noise points. The scanning process was 10 second interval between each steps. Each step was 1 μm. The third figure (lower left) is the re-building figure from the original data with X-axis corresponding to the scanning steps while the right figure is the figure of the scanning result with 1.5 pixels added together. By study the motion tracking figure, we could find out that each step length is close to 1.414 pixels. So we used 1.5 instead of 1.0 to add up the signals.

4 Conclusion and Future work

4.1 Conclusion

Fluorescence Nanoprobe was successfully fabricated and demonstrated in the image in nanostructures. Varies fiber taper pulling etching techniques were tested and used in the nanoprobe fabrication. Single MWCNT was controllable attached to the fiber taper tip. Chemical synthesis of core/shell structure of QD@SiO_2 was performed and results were showed. Covalent bonding of QDs to the surface of MWCNT was also carried out and QDs were bonded to the selected area (the tip) of the MWCNT. All these components were put together to make the fluorescence nanoprobes.

Nanoprobe fabrication system was integrated with the fluorescence detection and scanning systems, which made it easy to monitor the fabrication process in real time and break the optic diffraction limit. Liquid nitrogen cooled monochromator was used in the spectrum measurement which was sensitive to the weak signals.

4.2 Future Work

In the future, we still have a lot work to be done about the nanoprobe.

First, we will go on with work on the measurement of the nanoprobe. We have already bought a Picoharp 300, picoseconds two-channel time-correlated single photon counting system for the quantum dots life measurement.

The measurement scheme and the device image are shown above. The left is the life measurement setup, which comprise of a PDL pulse laser, quantum dots sample, PMT and the Picoharp single photon counting system. The right figure is the device picture and the lower one is the lift signal measurement plot.

Second, single photon source fabrication is capable under our present system. Right now, the single photon source was fabricated majorly by semiconductor processing method. But, with our system, we can control the quantity of the quantum dot connected to the surface of the SiO_2. If we could, at last, put only one quantum dot to the SiO_2, it would be

a perfect single photon source since only quantum dot would generate one photon a time with pulse excitation source.

4.3 Summary of contributions

--- Successfully chemical synthesis of core/shell QD@SiO_2 nanospheres

--- Covalently bonded the quantum dots to the end of MWCNT

--- Using fluorescence image to solve the problem of diffraction limit and applied to the nanoprobe fabrication

--- Design and integrated the nanoprobe fabrication system with the fluorescence detection system, which made it easy to catch the fluorescence spectra and performing scanning experiment.

Reference

1. D. M. Eigler and E. K. Schweizer, *Nature,* vol. 344, 524, 1990.
2. Y. Li, G. W. Meng, and L. D. Zhang, *Appl. Phys. Lett.*, vol.76, 2011, 2000.
3. M. H. Huang, S. Mao, et al, *Science*, vol. 292. No. 5523, 1897, 2001.
4. Y. Huang, Y. Cui, and C. Lieber*, NANO LETTERS*,vol. 2, No. 2,101, 2002.
5. P. Michler, A. Imamoglu, et al, *Science,* vol. 290. no. 5500, 2282, 2000.
6. C. B. Murray, C. R. Kagan, M. G. Bawendi, *Science,* vol. 270. No. 5240, 1335, 1995.
7. M. S. Dresselhaus, G. Dresselhaus, J. C. Charlier, E. Hernández, Phil. Trans. R. Soc. Lond. A 2065, 2004.
8. M. Yu, *Phys. Rev. Lett.* , vol.84, 5552, 2000.
9. K. Brunner, U. Bockelmann, G. Abstreiter, M. Walther, G. Böhm, G. Tränkle, and G. Weimann, *Phys. Rev. Lett.* vol.68, 3216, 1992.
10. L. Bakueva and S. Musikhin, *Appl. Phys. Lett.* vol. 82, 2895 2003.
11. T.H. SCHMIDT, G. J. SCHUTZ, W. BAUMGARTNER, H. J. GRUBER, AND H. SCHINDLER*, Proc. Natl. Acad. Sci. USA,* vol. 93, 2926, 1996.
12. W.Gan and J. Lichtman, et al., *Neuron*, vol. 27, 219, 2000.
13. M., Chalfie, Y. Tu, W.W. Ward, and D.C, Prasher, *Science*, vol. 263, 802, 1994.
14. A.N.van den Pol, and P.K.Ghosh, *J. Neurosci,* vol.18, 10640, 1998.
15. Jacob Fish, *Journal of Nanoparticle Research*, vol. 577, 2006.
16. P.J. Burke, Z. Yu, C. Rutherglen, *Carbon nanotubes for RF and microwaves*, 13th GAAS®Symposium – Paris, 2005.
17. K. Jensen, J. Weldon, H. Garcia, and A. Zettl, *NANO LETTERS,* vol. 7, No. 11,3508,2007.
18. J. Lee, H.W. Seol, et al., Proceedings of the 2nd IEEE International Conference on Nano/Micro Engineered and Molecular Systems, 254, 2007.
19. T. Vo-Dinh,P. Kasili and M. Wabuyele, *Nanomedicine: Nanotechnology, Biology, and Medicine*, 22, 2006.
20. P. G. Collins, A. Zettl, R. E. Smalley, *Science,* vol. 278. no. 5335, 100, 1997.
21. R.Soong, C. D. Montemagno, et al, *Science,* vol. 290. No. 5496, 1558, 2000.
22. R.Lüthi, R. Schlittler, J. Brugger, and P.Vettiger et al., *Appl. Phys. Lett.* 75, 1314, 1999.
23. D. W. Pohl, W. Denk, and M. Lanz, *Appl.Phys. Lett*. vol. **44**, 651, 1984.
24. A. Lewis, H. Taha, A. Strinkoviski, A. Manevitch, A. Khatchatouriants, R. Dekhter, and E. Ammann, *Nature Biotechnology*, vol. **21**, 1278, 2003.
25. D. Richards, *Phil. Trans. R. Soc.Lond. A*, vol. **361**, 2843, 2003.
26. S. Iijima, *Nature*, vol. 354, 391, 1991.
27. R. Baughman, A. Zakhidov, W. de Heer, *SCIENCE*, vol. 297, 787, 2002.
28. S. G. Louie*, Top. Appl. Phys.* Vol. 80, 113, 2001.
29. W. Liang et al, *Nature*, vol. 411, 665, 2001.
30. S. P. Frank, P. Poncharal, Z. L. Wang, W. A. de Heer, *Science*, vol. 280, 1744,1998.
31. P. Kim, L. Shi, A. Majumdar, P. L. McEuen, *Phys. Rev. Lett.* vol. 87, 215502, 2001.
32. G. Gao, T. C¸ag˘ın, W. A. Goddard, *Nanotechnology* vol. 9, 184, 1998.
33. M.-F. Yu, B. S. Files, S. Arepalli, R. S. Ruoff, *Phys. Rev. Lett.* vol. 84, 5552, 2000.
34. D. A. Walters et al, *Appl. Phys. Lett.* vol. 74, 3803, 1999.

35. E. W. Wong, P. E. Sheehan, C. M. Lieber, *Science*, vol. 277,1971-1975, 1997.
36. H. J. Dai, J. H. Hafner, A. G. Rinzler, D. T. Colbert, R. E. Smalley, *Nature*,vol. 384, 147,1996.
37. P. Kim, C. M. Lieber, *Science*, vol.286, 2148,1999.
38. M.G. Bawendi, M.L. Steigerwald, L.E. Brus, *Annual Review of Physical Chemistry*, vol. 41, 477, **1990**.
39. F Prieto1, L M Lechuga1, et al., *Nanotechnology*, vol.14, 907, 2003. G. M.
40. Whitesides and J. C. Love, Sci. *Am.,* 39, 2001.
41. G. S. Bales, A. C. Redfield, and A. Zangwill, *Phys. Rev. Lett.* vol. 62, 776, 1989.
42. http://cmxr.com/Industrial/Handbook/Chapter3.htm and http://cmxr.com/Industrial/Handbook/Chapter5.htm
43. Y. Kurokawa1, Y. Ohno, et.al, *Jpn. J. Appl. Phys.* vol.43, 5669, 2004.
44. S. J. Wilson and M. C. Hutley, *Optica Atca,* vol. 29, 993, 1982.
45. P. B. Clapham, and M. C. Hutley*, Nature,* Vol. 244, 281, 1973.
46. W. Barthlott and Neinhuis, *Planta,* 202, 1, 1997.
47. W. Barthlott*, Scanning electron microscopy of the epidermal surface in plants. In: D. Claugher (ed) Scanning electron microscopy in taxonomy and functional morphology,* Clarendon Press, Oxford, 69-94, 1990
48. W. Barthlott, *Epicuticular wax ultrastructure and systematics. In: Behnke HD, Mabry TJ (eds) Evolution and systematics of the Caryophyllales*. Springer*,* Berlin*,* 75-86, 1993
49. L. P. Biro, et,al., *Phys. Rev. E,* vol. 67, 021907, 2003.
50. Michael Gross, *Travels to the Nanoworld: Miniature Machinery in Nature and Technology*, 1999, reissued 2001.
51. Edward A. Rietman, *Molecular Engineering of Nanosystems*, Springer-Verlag New York Inc., 2001.
52. N. Seeman, *Nature*, vol. 421, 427, 2003
53. C. Niemeyer, *Angew. Chem. Int. Edn*, vol. 40, 4128, 2001.
54. C. Niemeyer, *Curr. Opin. Chem. Biol.,* vol. 4, 609, 2000.
55. J. Storhoff and C. Mirkin*, Chem. Rev.,* vol. 99, 1849, 1999.
56. V. Trubetskoy and J. Hagstrom, et al., *Nucleic Acids Research*, 4178, 1998.
57. E. Braun, and G. Ben-Yoseph, et al., *Nature*, vol. 376, 775, 1997.
58. S. Mann, W. Shenton, M. Li, S. Connolly, D. Fitzmaurice, *Advanced Materials,* vol. 12, 147, 1999.
59. K. Nam, A. Belcher, et al., *Science*, vol. 312, 885, 2006.
60. Chuanbin Mao, et al, *Science*, Vol. 303,213, 2004.
61. J.R. Arthur, *J. Appl.Phys.*, vol. 032, 1968.
62. F.Capasso, A.Cho, et, al, *Appl. Phys. Lett.,* Vol. 46, 664, 1985.
63. D. Gracias, G. Whitesides, *Appl.Phys. Lett*,, Vol. 80, 2802, 2002.
64. Geim, A. K. *et al*., *Nature Materials*, vol. 2, 461, 2003.
65. M. Phillips, *Detection of volatile organic compounds in breath Disease Markers in Exhaled Breath: Basic Mechanisms and Clinical Applications,* N Marczin and M Yacoub (London: Taylor and Francis) pp 219–31, 2002.
66. V. Arterbery and T. Risby, ey al., Biol. *Med.* Vol .17, 569, 1994.
67. K. Yum, and M. Yu,et alk., *ACS Nano*,vol. 1,NO. 5, 440-448 2007.

68. N. Fang,et al., International Conference on BioMedical Engineering and Informatics,619-623, 2008.
69. W. Tan, Z.Y. Shi, S. Smith, D. Birnbaum, and R. Kopelman, *Science,* vol 258, 778, 1992.
70. T .Vo-Dinh, et al, *Appl. Spectrosc*, vol. 41:735, 1987.
71. T. Vo-Dinh, et al, *Nanomedicine: Nanotechnology, Biology, and Medicine*, vol. 2 22, 2006.
72. P. Kasili, et al, *J Nanosci Nanotechnol,* vol. 2, 653, 2002.
73. T. Vo-Dinh T, et al, *Nature Biotechnol,* vol. 18,764, 2000.
74. T. Vo-Dinh, et al, *J Nanopart Res*, vol. 2, 17, 2000.
75. B. Cullum,et al., *Anal Biochem*, vol. 277, 25, 2000.
76. P. Kasili, et al, *J.Am.Chem. Soc.*, vol. 126, 2799, 2004.
77. M. Alencar, *Appl. Phys. Lett.,* vol .84, 4753, 2004.
78. B Samson1, *Journal of Physics: Conference Series*, vol. 92,012089, 2007.
79. A. Lewis, H. Taha, A. Strinkoviski, A. Manevitch, A. Khatchatouriants, R. Dekhter, and E. Ammann, *Nature Biotechnology,* vol. 21, 1278, 2003.
80. D. Richards, *Phil. Trans. R. Soc. Lond. A,* vol. 361, 2843, 2003.
81. Y. Xu, W. Liang, A. Yariv, J. G. Fleming, and S. Lin, *Opt. Lett.*, vol. 29, 424, 2004.
82. C. Brunel, and M. Orrit, et al., *Phys. Rev. Lett.*, vol. 83, 2722, 1999.
83. G. S. Solomon, M. Pelton, and Y. Yamamoto, *Phys. Rev. Lett.,* vol. 86, 3903, 2001.
84. A.S. Lapchuka, and A.A. Kryuchyn, *Ultramicroscopy*, vol.99, 143, 2004.
85. Z. Lu, *Phys. Rev. Lett. ,* vol. 95, 153901, 2005.
86. L. Quinti, R.Weissleder, C. H. Tung, *Nano Lett.*, vol. 6, 488 –490, 2006.
87. K. Kim, et al, *J. Am. Chem. Soc.* vol. 128, 3490, 2006.
88. S. I. Stoeva, J. S. Lee, J. E. Smith, S. T. Rosen, C. A. Mirkin, *J.Am. Chem. Soc*., vol. 128, 8378 – 8379, 2006.
89. Bruchez Jr., M.B. et al. *Science,* vol. 281, 2013, 1998.
90. H. Mattoussi, et al., *Journal of the Association for Laboratory Automation,* vol. 9, 28, 2004.
91. Y. Zhang, et al, *Analytical Biochemistry*, vol. 364(2), 122, 2007.
92. G.T. Shubeita, et al, *J. Microsc.,* vol. 210, 274, 2003.
93. L. Aigouy, et al, *Rev. Sci. Inst.* Vol. 77, 063702, 2006.
94. R. Zenobi, et al, *Appl. Phys. Lett.,* vol. 75,160, 1999.
95. K. Takechi, T. Eguchi, H. Kanoh, T. Ito, and S. Otsuki, IEEE TRANSACTIONS ON SEMICONDUCTOR MANUFACTURING, vol. 18, No. 3, 384, 2005.
96. H.Ren, et al., *Optics & Laser Technology*, vol. 39, 1025, 2007.
97. V. I. Klimov, et al, *Science*, vol. 290, 314, 2000.
98. W. Lamgbein, et, al, *Nano Letters,* vol. 1, 309, 2001.
99. J. D. Jackson, Classical Electrodynamics, 3rd Ed., John Wiley & Sons (1999).
100. P. Kim, C. M. Lieber, *Science*, vol. 286, 2148,1999.
101. A. F. Koenderink, M. Kafesaki, B. C. Buchler, and V. Sandoghdar, *Phys. Rev. Lett.,* vol. 95, 153904, 2005.
102. D. L. Carroll, P. Redlich, P. M. Ajayan, J. C. Charlier, X. Blase, A. De Vita, R. Car, *Phys. Rev. Lett.* vol. 78, 2811, 1997.
103. T. W. Ebbessen, P. M. Ajayan, H. Hiura, K. Tanigaki, *Nature*, vol. 367, 519, 1994.

104. J. Liu, A. Rinzler, H. Dai, J. Hafner, R. Bradley, P. Boul, A. Lu, T. Iverson,K. Shelimov, C. Huffman, F. Rodriguez-Macias, Y. Shon, R. Lee, D. Colbert, R. E. Smalley, *Science* vol. 280, 1253, 1998.
105. P. M. Ajayan, S. Iijima, *Nature*, vol. 361, 333, 1993.
106. S. C. Tsang, Y. K. Chen, P. J. F. Harris, M. L. H. Green, A simple chemical method of opening and filling carbon nanotubes, *Nature* vol. 372, 159, 1994.
107. E. Dujardin, T. W. Ebbesen, T. Hiura, K. Tanigaki, *Science,* vol. 265, 1850, 1994.
108. Pulickel M. Ajayan1 and Otto Z. Zhou, *Topics Appl. Phys.* Vol. 80, 391, 2001.
109. T. Trindade,P. OBrien, X. Zhang, *Chem. of Mater.,* vol. 9(2), 523, 1997.
110. P. Nair, et al. *Journal of Materials Chemistry*, vol. 12(9), 2722, 2002.
111. Sathyajith Ravindran, and Cengiz S. Ozkan, et al., *NANO LETTERS*, vol. 3, No. 4,447, 2003.
112. http://www.evidenttech.com/products/evidots.html